Multi-objective path planning for unmanned surface vehicle with currents effects

Dr. Yong Ma

Associate Professor of school of Navigation,

Hubei Key Laboratory of Inland Shipping Technology,

Wuhan University of Technology,

1178 Heping Road

Wuhan, Hubei, 430063, PR China

myongdl@whut.edu.cn

Prof. Mengqi Hu

Assistant Professor of Department of Mechanical and Industrial Engineering,

University of Illinois at Chicago,

Chicago, IL 60607, United States

mhu@uic.edu

Prof. Xinping Yan

Dean of National Engineering Research Center for Water Transport Safety,

Endowed chair in Transportation Engineering, Wuhan University of Technology,

1178 Heping Road

Wuhan, Hubei, 430063, PR China

xpyan@whut.edu.cn

Abstract

This paper investigates the path planning problem for unmanned surface vehicle (USV), wherein the goal is to find the shortest, smoothest, most economical and safest path in the presence of obstacles and currents, which is subject to the collision avoidance, motion boundaries and velocity constraints. We formulate this problem as a multi-objective nonlinear optimization problem with generous constraints. Then, we propose the dynamic augmented multi-objective particle swarm optimization algorithm to achieve the solution. With our approach, USV can select the ideal path from the Pareto optimal paths set. Numerical simulations verify the effectiveness of our formulated model and proposed algorithm.

Keywords: Unmanned surface vehicle, Multi-objective path planning, Currents, Dynamic augmented multi-objective particle swarm optimization

1. Introduction

Featuring agile controllability, strong autonomy, and powerful field operational advantages, unmanned surface vehicles (USVs) have been extensively studied in the civil and military fields [1–4]. USVs are valuable for handling conventional maritime cruise and emergency rescue activities [5]. The paramount challenge that USVs face is the safety navigation [6], referring to the planning of high-quality conflict-free paths for such USVs. To guarantee the reasonable operation and quick response of reconnaissance and search missions, the path planning problem for USVs has become indispensable and ever-increasingly important.

Path planning for USVs is a branch of classical path finding for robots, including automatic ground vehicles (AGVs) and unmanned aerial vehicle (UAVs) [7] moving in the environment with obstacles. Different from the previous path finding for AGVs [8, 9] and UAVs [10], generating an effective path for USVs is needed to optimally fulfill missions through the waters and satisfy generous constraints simultaneously. USV path planning is similar to the ship navigation problem reported in [11–13]. [11] planned the safest path for vessels to pass through mined waters. The velocity obstacles approach generates a cone-shaped obstacle in the velocity space and plans a near-optimal safe path for the USV [14]. The path with minimum travel time is achieved in [15], and the resultant path with minimum energy consumption is obtained in [16, 17].

It is reasonable to identify that generous works depict the path planning problem as a single objective optimization model in which the objective can be to find the shortest path, the smoothest path, the most economical path (with minimum travel time or minimum energy consumption), the safest path, etc. Actually, the path length, smoothness, economic cost and safety goals play critical roles in USV path planning problems. It is necessary to pursue the shortest, smoothest, most economical and safest paths when the path planning issues are concerned. Quite sensibly, we focus on USV path planning studies with an emphasis on the above four objectives. Meanwhile, as noted in [15], owing to the drift generated by the currents and the inherent motion constraints of the underactuated USV [5, 15, 18], the effects of the currents [16–19] cannot be omitted in the USV path planning process. It is essential that currents effects should be concerned within the multi-objective USV path planning problems. Consequently, USV path planning studies with an emphasis on these four objectives, either explicitly or implicitly are reviewed in detail.

Obtaining the shortest path from the designed initial point to the final destination has been the main target of enormous quantities of real-world engineering applications [20, 21]. Extensive attention has been paid to the shortest path planning problem in the robotics field, including USVs, AGVs and UAVs. The studies strived to generate paths that were conflict-free, with the obstacles represented by certain shapes in a simplified environment [5]. [22] stated that the shortest path can be found with modified incremental heuristic algorithms. [23]

formulated the global shortest path planning problem in a latticed environment as a single objective linear programming model and provided a novel label-correcting algorithm to study this model. Within the shortest path planning problems, the planning environment is oversimplified, and little attention has been paid to environmental effects.

By following a smooth path, a USV can avoid jerky motion and prolong the service life of its mechanical devices [22, 24]. With a smooth path, the navigation, guidance and control of the USV can be substantially guaranteed [22, 25]. In our previous studies [8, 20, 21], the optimal path was denoted by a highly smooth polynomial function and the path smoothness goal was realized automatically. An inadequacy of our previous work is that, owing to the lack of realistic maneuverability, the given paths are not applicable to engineering problems. During the navigation, guidance and control activities, the paths of the USV through the water are represented by line segments connected with a sequence of waypoints. It is critically necessary to choose the smoothest path for USV path planning problem. Meanwhile, formulation of the smoothest path goal should concern the practical usage of the USV.

The economical path of a USV can be evaluated in terms of travel time or energy consumption. With respect to long-term and high-energy-consumption voyages, time and energy savings become the foremost issues of the path planning problem. When engaging the activities, including transportation [26, 27], cruise [28], and scientific investigation [29], the vessels would favor the most economical path, lowering the travel time and energy expenditure significantly. The resultant paths with minimum energy consumption are obtained in [16, 17]. [16, 17] verified that the energy consumption of the USV was markedly affected by the currents. Combined with the time cost function and the planning techniques, the sliding wave-front expansion approach analytically guarantees the feasible time-minimum path in strong currents [15]. [15] is the first attempt to introduce reinforcement learning for planning the minimum-travel-time path in ocean currents, whereas the obstacles and the motion boundary are not considered. To improve the practicability of the planned path, many constraints including the effects brought by currents [15], the obstacles, and the motion boundaries, should be incorporated into the path planning model. Reducing sailing time and energy consumption becomes remarkably essential when the USV needs to travel for a long journey affected by the currents.

Generally, the obstacles, including surface and underwater structures, impede the safety of USV navigation. [8, 20, 21] treated the obstacles as circles or spheres in two-dimensional or three-dimensional space, respectively, and safety was embedded as a constraint of the path planning problem. [30] provided the safest path planning for planar robots wherein an interval value was used to represent the safety. Owing to the absence of an intuitive safety representation, their work is hard to apply in practice to address path planning issues. Without the safety guarantee, a USV cannot successfully execute missions or tasks. To make up for the above deficiency and highlight the importance of safety, this work strives to optimize the path safety in the USV path planning problem.

From the above literature review, referring to the path planning problem for USVs in environments with currents effects, it can be observed that the formerly developed models aim to optimize only one single objective. The path length, path smoothness, economic cost and path safety are all important objectives in our focused issue. To the best of our knowledge, less attention has been paid to the joint optimization of the shortest, smoothest, most economical and safest goals in USV path planning problems that are subject to current effects, especially considering the above four objectives simultaneously. When comes to the complexity of our focused problems, the above four goals are generally conflicting criteria of the path planning problem, within which they interrelate with and restricting each other in the optimization process. To bridge these research gaps, we propose a multi-objective path planning algorithm for USVs by explicitly taking into account various constraints, especially the effects brought by currents.

Since the 1990s, generous fruitful works have been achieved in the domain of path planning, accompanied by promising algorithms [8, 20, 21]. The algorithms are classified as classical approaches and heuristic approaches [8]. With its rigid procedures, a classical approach can achieve an optimal solution if one exists, whereas a heuristic approach can obtain the solution when classical approaches lose effectiveness. Genetic algorithms [31], simulated annealing and evolutionary algorithm [8] belong to the heuristic approach category. The particle swarm optimization (PSO) algorithm [8, 32–34] is subordinate to the heuristic approach and has the merits of simplicity, ease of implementation, and population-based evolutionary ability. Meanwhile, multi-objective PSO (MOPSO) algorithms have been developed for nearly two decades and have made considerable progress in tackling multi-objective optimization problems [35]. [30] adopted MOPSO to plan paths for robots and generated Pareto optimal paths. The fitness of MOPSO varies widely depending on the

complexity and dimensionality of the considered problems [35]. The simultaneously optimized objectives are often reciprocally restrained. Taking the current influence into account, the shortest path of the USV may not correspond to the economical optimal path. The shorter path would be reached at the expense of the path safety used to endure the adversities brought by the current. Consequently, we propose a dynamic augmented MOPSO (DAMOPSO) to generate the high-quality Pareto optimal paths set for the USV wherein the multiple objectives and many constraints are embodied.

Some highlights of our paper are: (1) we consider multiple optimized objectives, including the travel length, the smoothness, the economic cost, and the safety of the path for USV path planning problem. Many constraints, such as the motion limitations and the currents effects are considered in our study; (2) we formulate a multi-objective optimization model for the USV path planning problem under environments with currents; (3) after analyzing the characteristics of the model, we introduce an algorithm DAMOPSO to conduct a trade-off analysis among the four objectives. Finally, simulations with different scenarios verify the effectiveness of the USV path planning model.

The remainder of the paper is organized as follows. Section 2 describes the USV path planning problem formulation. Section 3 analyzes the multi-objective model characteristics and proposes a solution approach DAMOPSO to resolve the problem. Section 4 presents illustrative numerical examples for USV path planning using the proposed approach. Finally, Section 5 concludes this paper.

2. Problem formulations

To expressly formulate the multi-objective path planning problem for unmanned surface vehicle with currents effects, this section presents the nomenclatures of the motion model and environment of the USV, our focused four objectives, and constraints. Following that, we sequentially illustrate the USV motion model, motion environment, and the multiple objectives of USV path planning in detail.

Nomenclature related to the USV motion model	
m_{USV}	mass of the USV
u	surge speed
v	sway speed
$\dot{u}$	corresponding acceleration of u
$\dot{v}$	corresponding acceleration of v
r	yaw rate
$\dot{r}$	yaw acceleration
x_G	center of gravity abscissa
X	the force acted on USV's heading directions
Y	the force acted on USV's abeam directions
I_z	the yaw moment of inertia of the USV
N	yaw moment

Nomenclature related to motion environment	
Bounded motion area	
s_i	elementary line segment, $i = 1, \ldots, m$
S	USV's path, $S = \cup_{i=1}^{m} s_i$, $i = 1, \ldots, m$
(x_0, y_0)	initial location
(x_f, y_f)	the intended final position
k	the number of obstacles
O_{bs_j}	the jth obstacle, $j = 1, 2, \ldots, k$
O_{bs}	set of obstacles
C_{han}^{L}	linear left boundary of the channel
C_{han}^{R}	linear right boundary of the channel
C_{han}	boundaries of the channel
A_{rea_free}	obstacle-free motion area
Effects of currents on path planning	
$\phi(x, y)$	mathematical model of the time-varying currents
$B(t)$	oscillation of the meander amplitude
v_c	velocity of the currents
v_{cx}	v_c on the OX direction
v_{cy}	v_c on the OY direction
V	velocity of the USV
θ	USV's heading angle related to OX direction
V_x	USV's velocities projected on OX direction
V_y	USV's velocities projected on OY direction

Nomenclature related to multi-objectives	
The shortest path length	
objective 1	min $L_0 = \sum_{i=1}^{m} s_i$
δ	a certain step that the x-coordinate of S divided by
The smoothest path	
objective 2	min $\theta_0 = min(max(\zeta_i))$
θ_{si}	turn angle between (x_{si-1}, y_{si-1}) and (x_{si}, y_{si})
ζ_i	turn angles between s_i and s_{i+1}
pi	the value of π
The minimum economic cost path	
objective 3	min $E_0 = \sum_{i=1}^{m} \frac{s_i}{V+v_c} FCPUT$
T_0	the travel time of the path
E_0	the energy consumption of the path
$FCPUT$	fuel consumption per unit time (kg/h)
The safest path	
objective 4	min $D_{Safe} = \sum_{j=1}^{k} D_{Safej}$
L_{USV}	USV's length
(x_{ccj}, y_{ccj})	center of a circle corresponding to O_{bs_j}
r_{ccj}	radius of a circle corresponding to O_{bs_j}
d_{real_j}	real distance between O_{bs_j} and S
d_{safe_minj}	the least distance between O_{bs_j} and S
d_{safe_maxj}	the lower limit of the maximum distance between O_{bs_j} and S
D_{safej}	safety degree of S related to O_{bs_j}

Nomenclature related to constraints	
Motion boundaries constraints	
(x_{s0}, y_{s0})=(x_0, y_0)	constraint of initial location
(x_{sm}, y_{sm})=(x_f, y_f)	constraint of final location
Obstacle-avoidance criteria	
$S = \cup_{i=1}^{m} s_i \subset A_{rea\_free}$	planned paths fall in obstacle-free motion area
Velocity constraints	
$V_x = Vcos\theta + v_{cx}$	currents effects on OX direction
$V_y = Vsin\theta + v_{cy}$	currents effects on OY direction
$V + v_c \geq 0$	constraint of velocity

2.1. The USV motion model

Appropriate knowledge of the maneuvering behavior of the USV contributes to the path planning problem. To study the maneuverability of the USV, it is necessary to reflect the motion of six degrees of freedom in the mathematical model [36]. Generally, within the path planning problem, the navigation of the USV can be treated as a rigid body motion on the horizontal surface in the form of three degrees of freedom (the surge, sway and yaw), thus neglecting heave, roll and pitch motions. Detailed motion equations of the USV can refer to [36, 37]. The coupled surge-sway-yaw model of the USV is

$$\begin{cases} m_{USV}(\dot{u} - vr - x_G r^2) = X & Surge \\ m_{USV}(\dot{v} + ur + x_G r^2) = Y & Sway \\ I_Z \dot{r} + m_{USV} x_G (\dot{v} + ur) = N & Yaw \end{cases} \tag{1}$$

2.2. Motion environment of the USV

2.2.1. Bounded motion area of the USV

Suppose the USV's path S consists of a sequence of linked elementary line segments s_i $(i = 1, \ldots, m)$. Following path S, USV navigates from the initial location (x_0, y_0) to the intended final position (x_f, y_f) in the presence of a set of obstacles O_{bs} $(O_{bs} = \{O_{bs\_1}, O_{bs\_2}, \ldots, O_{bs\_j}, \ldots, O_{bs\_k}\}$, $j = 1, 2, \ldots, k$, and k is the number of obstacles). The obstacles including over-water buildings and submerged obstructions are represented as polygons on the horizontal plane. Meanwhile, the boundaries of the channel C_{han} are composed of the linear left boundary C_{han}^L and right boundary C_{han}^R. The boundaries of the channel C_{han} can be expressed as

$$C_{han} = C_{han}^L \cup C_{han}^R, \qquad C_{han}^L, C_{han}^R \subset R^2 \tag{2}$$

In Eq. (2), the two-dimensional variables C_{han}^L and C_{han}^R together represent the boundaries of the channel C_{han}.

The bounded obstacle-free motion area of the USV is calculated as follows

$$A_{rea\_free} = C_{han} - O_{bs} = C_{han}^L \cup C_{han}^R - \cup_{j=1}^{k} O_{bs\_j} \tag{3}$$

In Eq. (3), if taking into consideration USV's collision-avoidance motion with obstacles, O_{bs} should be cut out from C_{han}, and then reached the bounded obstacle-free motion area A_{rea_free} of USV. Accordingly, to guarantee the safety, the generated path should be restricted to A_{rea_free}. The path S should be

$$S = \cup_{i=1}^{m} s_i \subset A_{rea\_free} \tag{4}$$

It is observed from Eq. (3-4) that USV cannot collide with obstacles and should be bounded in the obstacle-free area A_{rea_free}. Once the path S crosses the area with obstacles, there is no doubt that the planned path is dangerous for the USV and should be discarded.

2.2.2. Effects of currents on path planning for the USV

Many studies have addressed effects of currents on path planning for the USV [5, 15, 15, 18]. [16–19] mainly considered the energy-saving path planning problem with currents influence. [38] analytically found feasible and optimal path in a strong current field by using a novel sliding wavefront expansion approach.

These demonstrate that many studies lay stress on energy saving for path planning in the current environment. To ensure operational efficiency for USVs under currents effects, it is necessary to plan high-quality path considering multiple objectives, including the minimum path length, path smoothness, energy/time savings and path safety. In this research, we will consider two types of currents: those with fixed speed and direction, and those with time-varying distributions. Currents with fixed speed and direction [15] are appropriate for inland voyaging, while the time-varying currents can be applied to coastal and ocean voyaging. To reflect the large-scale ocean chaos transparently, the currents with time-varying distribution are represented by an eastward flowing jet, which is depicted using a mathematical model with north-south directional meandering as below [19, 39].

$$\phi(x,y) = 1 - \tanh\left(\frac{y - B(t)\cos(k(x-ct))}{\left(1 + k^2 B(t)^2 \sin^2(k(x-ct))\right)^{1/2}}\right) \quad (5)$$

In Eq. (5), a time-dependent dimensionless function $B(t)$ represents the oscillation of the meander amplitude, which can be expressed as $B(t)=B_0 + \epsilon\cos(\omega t + \beta)$. B_0, ϵ, ω, β, k and c are adopted to illustrate the time-varying current field that is updated at each integrate value of time [19]. Suppose components of the current velocity v_c in the directions of OX and OY in XOY coordinates are v_{cx} and v_{cy}, respectively. Then, at time t, v_{cx} and v_{cy} can be computed as

$$\begin{cases} v_{cx}(t) = -\dfrac{\partial\phi}{\partial y} \\ v_{cy}(t) = \dfrac{\partial\phi}{\partial x} \end{cases} \quad (6)$$

As expounded above, the effects of currents should be strengthened from the perspective of the direction and magnitude of the current velocity in USV path planning. In Fig. 1, the boundaries of the left and right channel are shown as a sequence of line segments in the color of blue and red, respectively. The dark curves with arrows distributed from left to right represent currents. The red evenly shaped pentagon denotes the USV, and S_1 and G_1 stand for its start and final positions, respectively. Suppose that, at S_1, the velocity of the USV is V and the heading angle related to the direction of OX is θ. The effects exerted on the USV by currents would be evidently manifested in the velocity of the USV. Suppose V_x and V_y are the velocities of the USV projected on the OX and OY directions; they are calculated as

$$\begin{cases} V_x = V cos\theta + v_{cx} \\ V_y = V sin\theta + v_{cy} \end{cases} \quad (7)$$

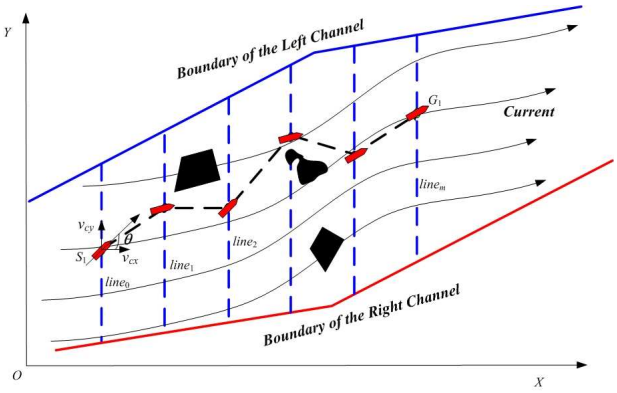

Figure 1: Path planning scheme for the USV

As shown in Fig. 1, the motion of the USV is forward and toward to the destination. Even under the severe condition that the USV travels along the reverse direction of the current, this work postulates that the USV could endure the potential negative effect brought by the current, and the below constraints should be satisfied

$$V + v_c \geq 0 \quad (8)$$

2.3. Multiple objectives of USV path planning

Referring to the USV, the shortest path length contributes to its task and mission complement; the much smoother path benefits its maneuverability; the energy- and time-saving path does great deeds for long-term and energy-demanding voyaging; the safest path can ensure that the USV executes activities with the highest safety. During the navigation process, the USV favors the safest path fully taking advantage of the currents, having great smoothness, and minimizing the travel length. Consequently, four objectives involving path length, path smoothness, economic cost, and path safety should be put forward to assess the path quality.

2.3.1. The shortest path length

Fig. 1 demonstrates that path S consists of several sequential line segments s_i $(i = 1, \ldots, m)$ from $S_1(x_0, y_0)$ to $G_1(x_f, y_f)$. Suppose that the x-coordinate of S is divided equally by a certain step δ, and that S is crossed with $m+1$ parallel line segments $line_j$ $(j = 0, 1, \ldots, m)$; then, the x-coordinate of s_i is increased orderly from s_1 to s_m with $x_{si} = x_0 + i\delta$ $(i = 1, \ldots, m)$, and the y-coordinate y_{si} of s_i falls on the y-coordinate of the line $line_i$ $(i = 1, \ldots, m)$.

Definition 1. *Suppose* x_{s0}=x_0, y_{s0}=y_0, x_{sm}=x_f, *and* y_{sm}=y_f. *We denote the path length by* L_0, *then* L_0=$\sum_{i=1}^{m} s_i$ =$\sum_{i=1}^{m} \sqrt{(x_{si} - x_{si-1})^2 + (y_{si} - y_{si-1})^2}$.

Consequently, the shortest path length objective can be defined as

$$min \quad L_0 \tag{9}$$

2.3.2. The smoothest path

The smoother the path is, the less turning maneuvers are required by the USV. It is an effective way to strengthen the maneuverability of the USV with a smooth path.

Definition 2. *Let* θ_{si+1}=$atan\left((y_{si+1}-y_{si})/(x_{si+1}-x_{si})\right)$ *and* θ_{si}= $atan\left((y_{si}-y_{si-1})/(x_{si}-x_{si-1})\right)$. *Continuous turn angles between* s_i *and* s_{i+1} *(i=1,...,m − 1) within the path* S *is denoted as* ζ_i. *Then,* ζ_i = abs $(\theta_{si+1}-\theta_{si})$*180/pi.

To promote the flexibility of the USV, ζ_i $(i = 1,\ldots,m-1)$ within the path S should be as small as possible. Following that, to evaluate the smoothness of the planned path, the maximum value of the turn angle set $\{\zeta_i, i = 1,\ldots,m-1\}$ is adopted to assess the path smoothness extent for the USV. Suppose θ_0=$max(\zeta_i)$. Accordingly, the smoothest path criterion can be

$$min \quad \theta_0 \tag{10}$$

2.3.3. The minimum economic cost path

To reduce the energy consumption, the USV could maintain its heading in accordance with the direction of currents and enlarge its velocity related to the ground as much as possible. To maximize the engine efficiency, [18] assumed that the output power of the engine is constant and that the USV should only be allowed to proceed toward the goal position. Consequently, the energy consumption of the path equals the travel time multiplied by the engine power of the unit time.

Definition 3. *Let* T_0 *be the travel time of the path, the value of* T_0 *is* $\sum_{i=1}^{m} s_i/(V+v_c)$.

Definition 4. *Let* E_0 *be the energy consumption of the path, and* $FCPUT$ *be the fuel consumption per unit time* (kg/h), *then* $E_0 = \sum_{i=1}^{m} s_i/(V+v_c)FCPUT$.

Remark 1. Taken into account E_0=$T_0 * FCPUT$, then the path with the least travel time coincides with the path with minimum energy consumption. Thus, the path with minimum economic cost corresponds to the path with the least travel time or the path with minimum energy consumption.

Consequently, the most economical planned path with minimum energy consumption or least time goal is obtained as follows

$$min \quad E_0 \tag{11}$$

2.3.4. The safest path

During the navigation process, the USV should pass through navigable waters without colliding with any obstacles. To ensure the safety of the USV, it is critical to achieve the safest path by which the USV can move freely from its start position to the final position. The bounded obstacle-free motion area of the USV is depicted in Section 2.2.1. The resultant path is only just conflict-free even though the obstacle-free constraints listed in Eq. (4) are satisfied. However, how to reveal the safety degree of the above path is up in the air. Because obstacles are represented by polygons, we propose the use of minimum circles that just cover the obstacles to embody the path safety degree. Suppose that the length of the USV is L_{USV}, that the set of the circles corresponding to k obstacles is $\{(x_{ccj}, y_{ccj}), r_{ccj}\}$, where k is the number of O_{bs}, $j = 1, 2, \ldots, k$, and that (x_{ccj}, y_{ccj}) and r_{ccj} are the center and the radius of the circle, respectively. The real distance, the least distance, and the lower limit of the maximum distance between O_{bs_j} and S are denoted as d_{real_j}, d_{safe_minj} and d_{safe_maxj}, respectively. The value of d_{safe_minj} is linear with L_{USV} and r_{ccj}. And the value of d_{safe_maxj} is also linear with L_{USV} and r_{ccj}. Then, when comes to the path S in Eq. (4), the safety degree of S related to the jth obstacle named D_{safej} is defined as

$$D_{Safej} = \begin{cases} 1 & d_{real\_j} \le d_{safe\_minj} \\ 0 & d_{real\_j} \ge d_{safe\_maxj} \\ \dfrac{d_{real\_j} - d_{safe\_minj}}{d_{safe\_maxj} - d_{safe\_minj}} & other \end{cases} \tag{12}$$

Definition 5. *Let* D_{Safe} *be the path safety. Then, safety degree of the path related to* O_{bs} *can be the sum of* D_{safej}. *Then,* $D_{Safe} = \sum_{j=1}^{k} D_{safej}$.

To plan the safest path, the following path safety objective should be optimized

$$min \quad D_{Safe} \tag{13}$$

Remark 2. Let p_{ath_1}, p_{ath_2} be the paths with the minimum L_0 and D_{safe}, respectively. p_{ath_1} corresponds to the optimal solution of Eq. (9), while p_{ath_2} corresponds to the optimal solution of Eq. (13). According to Definition 5, the value of D_{safe} in p_{ath_1} would be relatively larger than that in p_{ath_2}. Then, p_{ath_1} would not coincide with p_{ath_2}.

2.4. The formulated path planning model for the USV

By using the optimized planned path in terms of multiple objectives, including shortest path length, smoothest path, minimum economic cost and safest

path criteria, the USV could navigate freely within the boundaries of the channel and not collide with the obstacle set O_{bs}. Meanwhile, the influence of the currents, the motion boundaries and the dynamic constraints should be explicitly taken into account. Consequently, our multi-objective path planning model with many constraints for the USV is summarized as follows

$$min \quad L_0 = \sum_{i=1}^{m} s_i \tag{14}$$

$$min \quad \theta_0 = min(max(\zeta_i)) \quad i = 1, \ldots, m-1 \tag{15}$$

$$min \quad E_0 = \sum_{i=1}^{m} \frac{s_i}{V + v_c} FCPUT \tag{16}$$

$$min \quad D_{Safe} = \sum_{j=1}^{k} D_{Safej} \tag{17}$$

$$s.t. \begin{cases} (x_{s0}, y_{s0}) = (x_0, y_0) \\ (x_{sm}, y_{sm}) = (x_f, y_f) \\ S = \cup_{i=1}^{m} s_i \subset A_{rea\_free} \\ V_x = V cos\theta + v_{cx} \\ V_y = V sin\theta + v_{cy} \\ V + v_c \geq 0 \\ s_i = \sqrt{(x_{si} - x_{si-1})^2 + (y_{si} - y_{si-1})^2} \\ \zeta_i = \dfrac{abs\,(\theta_{si+1} - \theta_{si}) * 180}{pi} \quad i = 1, \ldots, m-1 \\ \theta_{si} = atan\left(\dfrac{y_{si} - y_{si-1}}{x_{si} - x_{si-1}}\right) \quad i = 1, \ldots, m \\ D_{Safej} = \begin{cases} 1 & d_{real\_j} \leq d_{safe\_minj} \\ 0 & d_{real\_j} \geq d_{safe\_maxj} \\ \dfrac{d_{real\_j} - d_{safe\_minj}}{d_{safe\_maxj} - d_{safe\_minj}} & other \end{cases} \end{cases} \tag{18}$$

Referring to Eq. (14-18), we optimize the path length listed in Eq. (14), path smoothness formulated as Eq. (15), economic cost given in Eq. (16), and path safety represented by Eq. (17) simultaneously. Meanwhile, the constraints are composed of the motion boundaries (the first two lines of Eq. (18)), obstacle-avoidance criteria (the succeeding line of Eq. (18)), effects of the currents (the fourth to sixth lines of Eq. (18)). And the expressions of several variables also embedded into Eq. (18), including the ith linear path length s_i ($i = 1, \ldots, m$) (the seventh line of Eq. (18)), the safety degree of S related to the jth obstacle D_{Safej} ($j = 1, \ldots, k$) (the rest of Eq. (18)). Then, the planned path for the USV satisfies with the above constraints and achieves a moderate balance among the multiple objectives.

Details of the variables in our formulated multi-objective path planning model are expounded as below. As shown in Eq. (14-17), the decision variables of the model are the x-coordinate x_{si} and the y-coordination y_{si} of the ith line segment s_i, where $(x_{si}, y_{si}) \subset C_{han}$, x_{s0}=x_0, y_{s0}=y_0, x_{sm}=x_f, y_{sm}=y_f, $i = 1, \ldots, m$. For the first objective, its variables are s_i, x_{si}, y_{si} and i, where s_i is the line segment between (x_{si-1}, y_{si-1}) and (x_{si}, y_{si}), $i = 1, \ldots, m$. For the second objective, its variables are ζ_i, θ_{si}, x_{si}, y_{si} and i, where ζ_i and θ_{si} are reached with the expressions listed in Eq. (18). For the third objective, its variables are s_i, V, v_c, $FCPUT$ and i, where the value of $FCPUT$ is a constant, and then V can be determined by $FCPUT$, and v_c can be obtained from Eq. (5-6). For the fourth objective, its variables are D_{Safej}, d_{real_j}, d_{safe_minj}, d_{safe_maxj} and j, where d_{real_j} is the Euclidean distance between the path S of USV and the jth obstacle O_{bs_j}, d_{safe_minj} and d_{safe_maxj} are constants for one certain USV, and O_{bs_j} ($j = 1, \ldots, k$) denotes the jth obstacle. As demonstrated by Section 2.3, the boundaries of above four objectives can be $0 \leq L_0 < \infty$, $0 \leq \theta_0 \leq 90°$, $0 \leq E_0 < \infty$, and $0 \leq D_{Safe} \leq k$, where k is the number of obstacles.

3. Dynamic augmented multi-objective particle swarm optimization algorithm for USV path planning

3.1. Analysis of model characteristics

As illustrated in Eq. (14-18), four nonlinear objectives, the constraints, such as the dynamic motion and obstacle-avoidance limitations, and the effects brought by the currents are explicitly considered.

Characteristic 3-1 Our formulated model features are time-varying and nonlinear.

Referring to the kinematics constraints and the currents effects, the optimal objectives including the path length, the path smoothness, the economic cost and the path safety, it is seen that the essence of the formulated multi-objective optimization path planning model for the USV is a time-varying nonlinear programming problem with many constraints and multiple optimal goals.

Characteristic 3-2 Our concerned path planning problem is NP-Hard.

The path planning problem has been classified as an NP-Hard problem [40], even the path planning case in the simplified horizontal plane [41, 42]. Our considered path planning problem for the USV with multiple objectives is subordinate to the NP-Hard problem set.

3.2. Brief states on MOPSO

To augment/enhance the performance of MOPSO, lots of studies tend to introduce generous techniques,

including the non-dominated sorting and sharing approach to maintain non-dominated solutions [43], the hyper-cubes based adaptive grid technique to achieve ideal Pareto frontier [44], and enhance the capacity of MOPSO modules [45, 46]. Above variants of MOPSO can be classified into the augmented/enhanced MOPSO.

Taking into account our focused time-varying and nonlinear problem, we introduce an approach named dynamic augmented MOPSO (DAMOPSO), within which the dynamic characteristic has been embodied. DAMOPSO consists of a PSO module, intelligent search method module, archive and leader dynamic update module, and path selection strategy.

Referring to DAMOPSO, by employing intelligent search method, the particle would be kept or discarded dynamically. By introducing an external archive, the size of the non-dominated solution and particle's leaders are updated dynamically. With the aid of correlation degree identification and path selection strategy, the correlations of our focused multiple objectives can be identified intelligently.

Difference between augmented/enhanced MOPSO and DAMOPSO is that, the dynamic characteristic is highlighted in the latter algorithm. To validate the effectiveness of our proposed DAMOPSO, we would compare with other MOO algorithms by using benchmark problems. Furthermore, USV path planning simulations under different scenarios are employed to validate the performance of our algorithm.

3.3. DAMOPSO algorithm

The fundamental steps of DAMOPSO are presented as follows. In addition, the parameters of DAMOPSO suitable for our path planning problem are depicted.

3.3.1. Particle encoding of DAMOPSO

In PSO, with M particles, particle m_p $(1 \le m_p \le M)$ stands for one potential solution of the given problem in D-dimensional space. Each particle m_p has three vectors at the lth iteration: the current position vector $u_{mp}(l) = (u^1_{mp}(l), u^2_{mp}(l), \ldots, u^D_{mp}(l))$, the velocity vector $V_{mp}(l) = (V^1_{mp}(l), V^2_{mp}(l), \ldots, V^D_{mp}(l))$, and its own best position vector $pBest = (p^1_{mp}, p^2_{mp}, \ldots, p^D_{mp})$, which represents the best objective function value or fitness value it has found thus far. One global best position vector $gBest = (p^1_g, p^2_g, \ldots, p^D_g)$ is defined as the position of the best particle among the M particles in the population. When all the terms are stated, the standard PSO formula [8] is given as

$$\begin{cases} V^d_{mp}(l+1) = wV^d_{mp}(l) + c_p r_{and\_1}(p^d_{mp} - u^d_{mp}(l)) + c_g r_{and\_2}(p^d_g - u^d_{mp}(l)) \\ u^d_{mp}(l+1) = u^d_{mp}(l) + V^d_{mp}(l+1) \qquad d = 1, 2, \ldots, D \end{cases} \tag{19}$$

In Eq. (19), the upper equation standardizes the movement update of particle m_p in dimension d at iteration number $l+1$, where w is a factor that controls the magnitude of V^d_{mp}, c_p and c_g are positive acceleration coefficients, and r_{and_1} and r_{and_2} are uniform random numbers in [0,1]; the lower equation gives the corresponding position $u_{mp}(l+1)$ update of particle m_p. Customarily, as in [47], we set the parameters to c_p=c_g=1 and w=0.8.

Section 2.3.1 states that the path S from $S_1(x_0, y_0)$ to $G_1(x_f, y_f)$ consists of a sequence of line segments s_i $(i = 1, \ldots, m)$ and is crossed with $m+1$ parallel line segments $line_j$ $(j = 0, 1, \ldots, m)$. The x-coordinate x_{si} of s_i is given in advance, while the y-coordinate y_{si} is unknown. Suppose the particle is denoted as $(y_0, y_{si}, \ldots, y_f)$, where y_{si} $(i = 1, \ldots, m, y_{im} = y_f)$ should be determined by DAMOPSO. Each particle plus $(x_0, x_{si}, \ldots, x_f)$ $(i = 1, \ldots, m, x_{im} = x_f)$ represents one potential path solution for the USV from $S_1(x_0, y_0)$ to $G_1(x_f, y_f)$. Then, the path S can be reached by linking (x_{si}, y_{si}) from $S_1(x_0, y_0)$ to $G_1(x_f, y_f)$ in order.

3.3.2. Intelligent search method

At each iteration, the values of the fitness functions $\{f_i\}$ $(i = 1, \ldots, 4)$ of each particle correspond to our four concerned objectives, and each particle is evaluated from the path feasibility and performance superiority over other particles. To enhance the performance of PSO, a weighted sum function f is introduced for each particle to select the $gBest$ from the external archive created in Section 3.3.3 with a minimum value of f. To promote the simplicity and practicability of our work, the weighted sum is shown as below.

$$f = \sum_{i=1}^{4} w_i f_i \tag{20}$$

where $w_i = r_i / \sum_{i=1}^{4} r_i$, r_i $(i = 1, \ldots, 4)$ randomly range from 0 to 1. Following that, the particle would be kept or discarded dynamically. The particle's best experience $pBest$ is updated based on the dominance relation between the current particle and the $pBest$ from the previous iterations.

3.3.3. Archive and leader dynamic update

Within the search process, the non-dominated solution with the maximum size N_{max} is maintained by introducing an external archive. The solutions existing in the external archive can be equivalent to the Pareto solutions that our algorithm has a tendency to fulfill. Following the multiple search methods module, the external archive and particle's leaders are updated dynamically. During the iteration process, a particle would

be added to the external archive if it dominates at least one solution that exists in the external archive, and the dominated solutions would be deleted from the external archive. As the number of the iterations increases, the size of the external archive is naturally enlarged, and the demand on computational time and space is overburdened. Consequently, a crowding distance is adopted to limit the archive size under N_{max} and retain the diversity of the external archive.

3.3.4. Correlation degree identification and path selection strategy

Referring to the optimal paths set reached by DAMOPSO algorithm, it is necessary to identify the correlations of our multi-objective. Inspired by the correlation analysis work in [48], the exact correlation coefficients coe_{cor} between two objectives are employed to demonstrate the correlations of our multiple objectives. For f_i, f_j, their correlation coefficients can be

$$coe_{cor}(f_i, f_i) = \frac{Cov(f_i, f_j)}{\sqrt{D(f_i)}\sqrt{D(f_j)}} \tag{21}$$

where $Cov(f_i, f_j)$ is the covariance of f_i and f_j, $\sqrt{D(f_i)}$ and $\sqrt{D(f_j)}$ are the variances of f_i and f_j, respectively, $(i, j = 1, \ldots, 4)$. There are 6 groups relations named the length versus the smoothness ($coe_{cor}(L_0, \theta_0)$), the length versus the economic cost ($coe_{cor}(L_0, E_0)$), the length versus the safety ($coe_{cor}(L_0, D_{safe})$), the smoothness versus the economic cost ($coe_{cor}(\theta_0, E_0)$), the smoothness versus the safety ($coe_{cor}(\theta_0, D_{safe})$), and the economic cost versus the safety ($coe_{cor}(E_0, D_{safe})$). The relationship between one objective and any other objective contributes to ascertain the correlation degree of any two objectives in our USV path planning problem. According to the value of coe_{cor} that falls in $[-1, 1]$, the lower the value, the higher the heterogenization of the two objectives, and vice versa.

In regard to above paths set, the USV should quickly select one reasonably efficient path. As demonstrated by [49], the tendency towards biased decision-making has been used to solve numerous complex preference problems successfully. Following that, weighted biased decision-making is employed to identify a path that the USV prefers to choose. A simple and efficient path selection strategy based on Min-Max Normalization is used to promote the path selection process for the USV. Values of the four objectives are normalized and transformed as val_{obj_ij}, where $val_{obj\_ij} \in [0,1]$, $i = 1, \ldots, 4$, $j = 1, \ldots, N_{path}$, and N_{path} is the number of paths in the set. Suppose that the preference pre_i $(i = 1, \ldots, 4)$ of the USV on each objective is equal to one random number in [0,1], that $\sum_{i=1}^{4} pre_i = 1$, and that the preference set $pre_{set}=\{pre_i\}$. Then, the ideal path for the USV corresponds to the one with the minimum processed prefer value (PPV), and PPV can be

$$PPV = \sum_{i=1}^{4} \sum_{j=1}^{N_{path}} val_{obj\_ij} * pre_i \tag{22}$$

Consequently, by virtue of simplification and the efficiency of the selection process, the USV can select the ideal path from the paths set with ease.

3.3.5. Parameters analysis

The swarm size N_{size} and the maximum iterations number T_{iter} should be set moderately, too large number of N_{size} and T_{iter} would occupy too much calculation space and affect the running speed, the small number of above two parameters would lead to reaching the low-quality solutions that out of our expectation. When the iteration number reaches to T_{iter}, the leaded results in the external archive with size N_{max} can be treated as our achieved Pareto optimal path solutions. According to the characteristics of our concerned problem and DAMOPSO algorithm, after testing and tuning the parameters many times, we set N_{size}=50, T_{iter}=200 and N_{max}=30. Determination details of the value of T_{iter} are expounded in Section 4.

3.4. Performance evaluation of DAMOPSO

To validate the effectiveness of our proposed DAMOPSO in the round, we execute the performance evaluation by using classical benchmark problems and MOO algorithms thoroughly. There are nineteen benchmark problems, including five ZDT (ZDT1, ZDT2, ZDT3, ZDT4 and ZDT6), seven DTLZ with two objectives (DTLZ1_2D, DTLZ2_2D, DTLZ3_2D, DTLZ4_2D, DTLZ5_2D, DTLZ6_2D and DTLZ7_2D), and seven DTLZ with three objectives (DTLZ1_3D, DTLZ2_3D, DTLZ3_3D, DTLZ4_3D, DTLZ5_3D, DTLZ6_3D and DTLZ7_3D). Details of the benchmark problems can be referred to [50]. The selected MOO algorithms are: archive-based hybrid scatter search (AbYSS), cellular differential evolution (CellDE), decomposition based MOPSO (dMOPSO), cellular genetic algorithm for MOO (MOCell), non-dominated sorting genetic algorithm II (NSGA-II), adaptive variation operator selection NSGA-II (NSGA-IIa), random variation operator selection NSGA-II (NSGA-IIr), optimized MOPSO (OMOPSO), and improved strength Pareto evolutionary algorithm (SPEA2). Above compared MOO algorithms are expatiated in [51–58].

In the light of general practice [50], the performance of the above algorithms can be reflected with the convergence and the diversity of the proximate Pareto frontier. Consequently, three indicators including additive unary epsilon indicator ($I^1_{\varepsilon+}$), spread (Δ), and hypervolume (HV) are addressed in our performance evaluation work. $I^1_{\varepsilon+}$ and Δ represent the convergence and the diversity performance, respectively. And HV indicates the convergence and the diversity jointly. It shows that smaller values are better for the first two indexes, and larger value is better for HV. Generally, to obtain necessary data for comparison, each algorithm runs independently 100 times, and N_{size} and N_{max} are set as 30 and 100, respectively. For two and three objectives problems, their maximum number of function evaluation is set to be 10 000 and 25 000, respectively. Details of above three indicators $I^1_{\varepsilon+}$, Δ and HV are shown in Table 1-3, respectively.

As shown in Table 1, from the perspective of $I^1_{\varepsilon+}$, DAMOPSO has better performance than a total of nine competitive MOO algorithms on eight out of nineteen benchmark problems. Meanwhile, referring to the other eleven benchmark problems, dMOPSO, SPEA2, AbYSS, and MOCell have slight advantages over other MOO algorithms. And DAMOPSO is highly competitive in comparison with above four best algorithms.

When comes to Δ, Table 2 indicates that DAMOPSO outperforms other nine MOO algorithms on four out of nineteen benchmark problems. Due to its best performance on the largest number of benchmark problems, DAMOPSO can be treated as the best algorithm.

Table 3 manifests that DAMOPSO has better performance that the nine excellent MOO algorithms on fifteen out of nineteen benchmark problems. Meanwhile, there are slight differences between values of DAMOPSO and values of the other four best algorithms. There is no doubt that DAMOPSO can be considered as the best algorithm in terms of HV.

By employing Wilcoxon test from the perspective of epsilon indicator $I^1_{\varepsilon+}$, spread Δ, and hypervolume HV [59], our obtained pairwise comparison results between DAMOPSO and other nine competitive algorithms are shown in Table 4. DAMOPSO has notably better performance on eight of nine MOO algorithms and is superior to dMOPSO validated by the indicator I^1_{ε}. As demonstrated by Δ, DAMOPSO is evidently superior to dMOPSO and outperforms other eight MOO algorithms. Meanwhile, DAMOPSO has remarkably better performance than all of the selected competitive MOO algorithms in terms of HV.

Consequently, with selected performance indicators $I^1_{\varepsilon+}$, Δ, and HV, our DAMOPSO has better performance than the nine competitive MOO algorithms. Due to its excellent performance, it is reasonable to resolve multi-objective USV path planning problems with DAMOPSO algorithm.

3.5. Path planning implementation based on DAMOPSO

3.5.1. Flow of DAMOPSO algorithm

By using the proposed DAMOPSO algorithm, according to the following generic steps, the multi-objective path planning for USV with currents effects can be tracked.

Algorithm *DAMOPSO*

Input: L_{USV}, (x_0, y_0), (x_f, y_f), O_{bs}, C_{han}, $\phi(x, y)$, V, f_i, c_p, c_g, w, N_{size}, T_{iter}, N_{max}, pre_{set}.
Output: $gBest$, S.
1 Draw the motion environment of the USV.
2 Formulate the mathematical model of the USV path planning problem by Eq. (14-18).
3 Set the parameters, including N_{size}, T_{iter}, and N_{max}.
4 Initial l=0, m_p, u_{mp}, V_{mp}, $pBest$ and $gBest$.
5 Calculate the circles that covered O_{bs} by method presented in [20].
6 Obtain the values of multiple objectives and the constraints in Eq. (14-18).
7 **If** $l \leq T_{iter}$, **Then**
8 Update u_{mp} and V_{mp} by Eq. (19).
9 Calculate $\{f_i\}$ $(i = 1, \ldots, 4)$ and constraints of Eq. (14-18).
10 Calculate f by Eq. (20).
11 Update $pBest$, $gBest$ according to the method introduced in Section 3.3.3.
12 l=l + 1.
13 **End If**.
14 Get the Optimal paths set $gBset$ for the USV.
15 USV select the suitable path from $gBset$ by Eq. (22).

3.5.2. Computational time complexity of DAMOPSO

Referring to the computational time complexity of DAMOPSO, it is notable that the time mainly generated from four parts of DAMOSPO, including a PSO module, intelligent search method module, archive and leader dynamic update module, and path selection strategy. The computational time complexity of a PSO module can be $O(T_{iter} \times N_{size} \times D \times N_f)$, where T_{iter} is the maximum iterations number, N_{size} is the swarm size, D is the spatial dimension, and N_f is the number of objectives. The computational time complexity of intelligent search method module can be $O(T_{iter} \times N_{size} \times N_f)$. When

Table 1: Median of the epsilon indicator $I^1_{\varepsilon+}$

	ZDT1	ZDT2	ZDT3	ZDT4	ZDT6	DTLZ1_2D	DTLZ2_2D
DAMOPSO	1.023E-02	9.886E-03	**6.968E − 03**	**1.038E − 02**	8.095E-03	**7.220E − 02**	1.086E-02
AbYSS	4.206E-02	6.155E-02	1.813E-01	6.604E-01	4.762E-02	4.206E+01	1.264E-02
CellDE	7.077E-02	4.805E-02	1.775E-01	9.251E+00	9.184E-03	1.413E+02	4.572E-02
dMOPSO	**8.129E − 03**	**6.549E − 03**	1.578E-02	1.256E-02	**5.179E − 03**	2.306E-01	1.128E-02
MOCell	2.092E-02	7.801E-02	5.754E-02	3.161E-01	6.165E-02	3.399E+01	**1.005E − 02**
NSGA-II	2.622E-02	6.441E-02	4.230E-02	8.058E-01	4.244E-01	4.730E+01	1.535E-02
NSGA-IIa	2.251E-02	7.513E-02	5.547E-02	1.688E+00	3.544E-01	1.284E+02	1.698E-02
NSGA-IIr	3.048E-02	7.947E-02	6.687E-02	1.031E+00	1.241E-02	1.132E+02	1.721E-02
OMOPSO	1.060E-02	8.844E-03	5.376E-02	8.224E+00	6.551E-03	1.449E+02	1.656E-02
SPEA2	4.402E-02	1.872E-01	7.534E-02	1.452E+00	6.818E-01	6.186E+01	1.383E-02
	DTLZ3_2D	DTLZ4_2D	DTLZ5_2D	DTLZ6_2D	DTLZ7_2D	DTLZ1_3D	DTLZ2_3D
DAMOPSO	**4.497E − 01**	3.339E-02	9.714E-03	9.792E-03	**8.825E − 03**	**1.321E − 01**	1.495E-01
AbYSS	1.212E+02	**1.251E − 02**	1.159E-02	8.340E+00	5.360E-02	3.280E+01	1.337E-01
CellDE	3.694E+02	7.370E-02	4.499E-02	2.359E+00	1.468E-01	1.106E+02	1.465E-01
dMOPSO	6.932E-01	4.035E-02	1.046E-02	**7.047E − 03**	1.078E-02	1.665E-01	1.345E-01
MOCell	9.500E+01	1.000E+00	**9.495E − 03**	6.167E+00	3.929E-02	5.710E+01	1.369E-01
NSGA-II	1.306E+02	1.578E-02	1.384E-02	8.104E+00	6.073E-02	4.432E+01	1.292E-01
NSGA-IIa	3.526E+02	1.890E-02	1.557E-02	6.214E+00	1.095E-01	9.552E+01	1.260E-01
NSGA-IIr	2.909E+02	1.774E-02	1.595E-02	3.848E+00	9.148E-02	8.608E+01	1.375E-01
OMOPSO	3.194E+02	2.361E-02	1.581E-02	8.327E-01	1.177E-02	8.875E+01	1.540E-01
SPEA2	1.717E+02	1.575E-02	1.377E-02	9.176E+00	1.445E-01	3.913E+01	**8.617E − 02**
	DTLZ3_3D	DTLZ4_3D	DTLZ5_3D	DTLZ6_3D	DTLZ7_3D		
DAMOPSO	**5.846E − 01**	1.633E-01	8.430E-03	**6.865E − 03**	1.729E-01		
AbYSS	9.085E+01	6.304E-01	**7.938E − 03**	8.553E+00	1.292E+00		
CellDE	2.858E+02	1.380E-01	6.352E-02	4.333E+00	7.783E-01		
dMOPSO	5.941E-01	2.547E-01	2.133E-02	1.940E-02	1.582E-01		
MOCell	1.172E+02	1.430E-01	8.711E-03	1.008E+01	2.866E-01		
NSGA-II	1.152E+02	1.176E-01	1.309E-02	7.636E+00	1.791E-01		
NSGA-IIa	2.632E+02	1.174E-01	1.327E-02	6.957E+00	1.466E-01		
NSGA-IIr	2.172E+02	1.285E-01	1.793E-02	3.117E+00	1.759E-01		
OMOPSO	2.956E+02	1.574E-01	1.780E-02	3.230E+00	2.660E-01		
SPEA2	1.309E+02	**9.067E − 02**	1.291E-02	7.444E+00	**1.328E − 01**		

Table 2: Median of the spread indicator Δ

	ZDT1	ZDT2	ZDT3	ZDT4	ZDT6	DTLZ1_2D	DTLZ2_2D
DAMOPSO	3.139E-01	3.014E-01	**7.237E − 01**	**2.767E − 01**	2.927E-01	**7.864E − 01**	2.942E-01
AbYSS	4.991E-01	6.612E-01	8.729E-01	9.666E-01	4.818E-01	8.768E-01	2.397E-01
CellDE	5.470E-01	5.128E-01	8.159E-01	9.659E-01	1.232E+00	8.709E-01	6.172E-01
dMOPSO	2.836E-01	**1.419E − 01**	1.016E+00	3.355E-01	**1.527E − 01**	1.480E+00	5.262E-01
MOCell	2.488E-01	3.052E-01	7.420E-01	8.272E-01	3.762E-01	8.554E-01	**2.246E − 01**
NSGA-II	3.657E-01	4.974E-01	7.528E-01	8.989E-01	7.244E-01	8.825E-01	3.855E-01
NSGA-IIa	3.653E-01	4.382E-01	7.644E-01	8.901E-01	7.153E-01	1.099E+00	3.957E-01
NSGA-IIr	3.948E-01	6.297E-01	7.879E-01	9.165E-01	7.219E-01	9.217E-01	4.416E-01
OMOPSO	**1.563E − 01**	1.427E-01	8.405E-01	9.318E-01	1.168E+00	8.095E-01	3.067E-01
SPEA2	4.371E-01	7.237E-01	7.623E-01	9.330E-01	8.078E-01	9.009E-01	3.355E-01
	DTLZ3_2D	DTLZ4_2D	DTLZ5_2D	DTLZ6_2D	DTLZ7_2D	DTLZ1_3D	DTLZ2_3D
DAMOPSO	8.814E-01	8.435E-01	3.001E-01	3.450E-01	5.846E-01	1.402E+00	6.637E-01
AbYSS	9.857E-01	**2.808E − 01**	2.401E-01	8.921E-01	7.812E-01	8.538E-01	7.832E-01
CellDE	8.770E-01	7.043E-01	6.260E-01	7.840E-01	7.453E-01	**6.825E − 01**	5.577E-01
dMOPSO	1.479E+00	1.253E+00	5.103E-01	**1.871E − 01**	7.519E-01	1.484E+00	8.945E-01
MOCell	9.950E-01	1.000E+00	**2.275E − 01**	8.637E-01	5.859E-01	7.854E-01	6.947E-01
NSGA-II	9.739E-01	4.074E-01	3.859E-01	8.629E-01	6.584E-01	8.341E-01	7.090E-01
NSGA-IIa	1.099E+00	4.269E-01	3.984E-01	9.675E-01	6.741E-01	9.168E-01	6.504E-01
NSGA-IIr	9.853E-01	4.637E-01	4.358E-01	8.893E-01	7.753E-01	8.041E-01	6.315E-01
OMOPSO	**7.655E − 01**	4.077E-01	3.115E-01	8.154E-01	**5.399E − 01**	7.663E-01	6.128E-01
SPEA2	9.851E-01	3.883E-01	3.380E-01	8.807E-01	7.911E-01	7.510E-01	**5.288E − 01**
	DTLZ3_3D	DTLZ4_3D	DTLZ5_3D	DTLZ6_3D	DTLZ7_3D		
DAMOPSO	1.533E+00	9.414E-01	2.899E-01	**3.049E − 01**	7.570E-01		
AbYSS	8.621E-01	5.675E-01	**1.886E − 01**	8.008E-01	6.895E-01		
CellDE	8.507E-01	5.596E-01	5.745E-01	7.366E-01	7.102E-01		
dMOPSO	1.524E+00	1.540E+00	8.069E-01	7.385E-01	1.149E+00		
MOCell	9.322E-01	7.071E-01	2.939E-01	6.975E-01	7.208E-01		
NSGA-II	9.896E-01	6.822E-01	4.929E-01	7.146E-01	7.619E-01		
NSGA-IIa	1.006E+00	6.574E-01	4.896E-01	8.656E-01	7.280E-01		
NSGA-IIr	8.689E-01	6.285E-01	5.765E-01	8.245E-01	7.268E-01		
OMOPSO	**7.804E − 01**	7.880E-01	5.929E-01	9.198E-01	7.056E-01		
SPEA2	1.016E+00	**5.384E − 01**	4.395E-01	5.533E-01	**6.055E − 01**		

Table 3: Median of the hypervolume indicator HV

	ZDT1	ZDT2	ZDT3	ZDT4	ZDT6	DTLZ1_2D	DTLZ2_2D
DAMOPSO	**6.613E − 01**	**3.281E − 01**	**5.157E − 01**	**6.607E − 01**	4.007E-01	**4.425E − 01**	**2.080E − 01**
AbYSS	6.244E-01	2.894E-01	4.848E-01	2.109E-01	3.529E-01	0.000E+00	2.060E-01
CellDE	5.683E-01	2.859E-01	4.122E-01	0.000E+00	4.007E-01	0.000E+00	1.615E-01
dMOPSO	6.614E-01	3.283E-01	5.133E-01	6.590E-01	**4.013E − 01**	3.413E-01	2.083E-01
MOCell	6.429E-01	3.160E-01	4.934E-01	5.468E-01	3.466E-01	0.000E+00	2.045E-01
NSGA-II	6.373E-01	2.873E-01	4.959E-01	1.065E-01	1.100E-01	0.000E+00	2.026E-01
NSGA-IIa	6.433E-01	2.821E-01	4.890E-01	0.000E+00	1.586E-01	0.000E+00	2.014E-01
NSGA-IIr	6.293E-01	2.777E-01	4.845E-01	0.000E+00	3.990E-01	0.000E+00	1.995E-01
OMOPSO	6.566E-01	3.256E-01	5.005E-01	0.000E+00	4.011E-01	0.000E+00	1.948E-01
SPEA2	6.177E-01	2.330E-01	4.812E-01	0.000E+00	2.296E-02	0.000E+00	2.000E-01
	DTLZ3_2D	DTLZ4_2D	DTLZ5_2D	DTLZ6_2D	DTLZ7_2D	DTLZ1_3D	DTLZ2_3D
DAMOPSO	**1.624E − 01**	**2.005E − 01**	2.095E-01	**2.118E − 01**	**3.342E − 01**	**6.724E − 01**	3.711E-01
AbYSS	0.000E+00	2.055E-01	2.076E-01	0.000E+00	3.015E-01	0.000E+00	3.754E-01
CellDE	0.000E+00	1.414E-01	1.643E-01	0.000E+00	2.538E-01	0.000E+00	2.857E-01
dMOPSO	1.243E-01	1.936E-01	**2.099E − 01**	2.118E-01	3.330E-01	5.732E-01	3.764E-01
MOCell	0.000E+00	0.000E+00	2.059E-01	0.000E+00	3.120E-01	0.000E+00	3.465E-01
NSGA-II	0.000E+00	2.020E-01	2.046E-01	0.000E+00	3.004E-01	0.000E+00	3.645E-01
NSGA-IIa	0.000E+00	1.981E-01	2.031E-01	0.000E+00	2.720E-01	0.000E+00	3.589E-01
NSGA-IIr	0.000E+00	1.974E-01	2.010E-01	0.000E+00	2.841E-01	0.000E+00	3.245E-01
OMOPSO	0.000E+00	1.870E-01	1.968E-01	0.000E+00	3.298E-01	0.000E+00	3.126E-01
SPEA2	0.000E+00	1.984E-01	2.013E-01	0.000E+00	2.622E-01	0.000E+00	**3.911E − 01**
	DTLZ3_3D	DTLZ4_3D	DTLZ5_3D	DTLZ6_3D	DTLZ7_3D		
DAMOPSO	**2.234E − 01**	3.410E-01	**9.316E − 02**	**9.464E − 02**	**2.809E − 01**		
AbYSS	0.000E+00	2.069E-01	9.315E-02	0.000E+00	2.485E-01		
CellDE	0.000E+00	2.826E-01	5.491E-02	0.000E+00	1.539E-01		
dMOPSO	1.885E-01	2.694E-01	9.077E-02	9.219E-02	2.416E-01		
MOCell	0.000E+00	3.449E-01	9.087E-02	0.000E+00	2.328E-01		
NSGA-II	0.000E+00	3.608E-01	9.111E-02	0.000E+00	2.625E-01		
NSGA-IIa	0.000E+00	3.579E-01	9.089E-02	0.000E+00	2.774E-01		
NSGA-IIr	0.000E+00	3.193E-01	8.789E-02	0.000E+00	2.633E-01		
OMOPSO	0.000E+00	2.995E-01	8.596E-02	0.000E+00	2.500E-01		
SPEA2	0.000E+00	**3.800E − 01**	8.849E-02	0.000E+00	2.645E-01		

Table 4: Wilcoxon test ($I^1_{\varepsilon+}$, Δ, and HV) between DAMOPSO and other 9 algorithms

DAMOPSO v.s.	Epsilon indicator $I^1_{\varepsilon+}$			Spread Δ			Hypervolume HV		
	R^+	R^-	$p-$value	R^+	R^-	$p-$value	R^+	R^-	$p-$value
AbYSS	180	10	**0.00062**	115	75	0.42091	181	9	**0.00054**
CellDE	185	5	**0.00029**	129	61	0.17124	189.5	0.5	**0.0002**
dMOPSO	136	54	0.09896	169	21	**0.00290**	157.5	32.5	**0.00956**
MOCell	175	15	**0.00128**	107	83	0.62916	186	4	**0.00025**
NSGA-II	168	22	**0.00331**	128	62	0.18418	182	8	**0.00050**
NSGA-IIa	164	26	**0.00549**	132	58	0.13650	183	7	**0.00040**
NSGA-IIr	168	22	**0.00331**	127	63	0.19783	190	0	**0.00013**
OMOPSO	168	22	**0.00331**	91	99	0.87212	189	1	**0.00016**
SPEA2	164	26	**0.00549**	114	76	0.44451	176	14	**0.00112**

comes to the archive and leader dynamic update module, its computational time complexity can be $O(T_{iter} \times N_{max} \times log(N_{max}))$ [51], where N_{max} is the maximum size of Pareto solutions. The computational time complexity of path selection strategy can be $O(N_f \times N_{max})$. Consequently, the computational time complexity of DAMOPSO can be $O(T_{iter} \times N_{size} \times D \times N_f) + O(T_{iter} \times N_{size} \times N_f) + O(T_{iter} \times N_{max} \times log(N_{max})) + O(N_f \times N_{max})$. Following that, when $N_{size} \times D \times N_f \geq N_{max} \times log(N_{max})$, the overall complexity of DAMOPSO algorithm can be $O(T_{iter} \times N_{size} \times D \times N_f)$. Otherwise, the overall complexity of DAMOPSO can be $O(T_{iter} \times N_{max} \times log(N_{max}))$. ?Generally, the value of N_{max} is less than the value of N_{size}, and when N_f is larger than 4, the value of $D \times N_f$ is evidently larger than the value of $log(N_{max})$. Following that, the complexity of our DAMOPSO algorithm with four objectives can be $O(T_{iter} \times N_{size} \times D \times N_f)$.

4. Computational simulations

Computational simulations under four different scenarios are provided to validate the performance of our formulated multi-objective path planning model. To balance the value of each objective, the value of the path cost E_0 is enlarged 10 times, and the value of the path safety D_{Safe} is also amplified 10 times. Suppose that L_{USV} = 92.6m, the length unit is the nautical mile (1 nmile = 1.852 km), and the velocity unit is the kn (1 kn =1 nmile/h). Then, the units of L_0, θ_0, E_0 and D_{safe} are nmile, °, h*10 and 1*10, respectively, where D_{safe} is dimensionless. Taking into account the relative scale of O_{bs} and the USV [1, 60, 61], we set the least distance d_{safe_mini} between O_{bs_i} and the path S of the USV equal to $L_{USV} + r_{cci}$ and the lower limit of the maximum distance d_{safe_maxi} between O_{bs_i} and the path S equal to $3L_{USV} + 1.8r_{cci}$, where r_{cci} is the radius of the circle that just cover the ith obstacle. The currents with fixed direction and speed are studied in the first two cases, while the time-varying currents are considered in the last two cases. With respect to the four optimal goals (the travel length, the smoothness, the economic cost and the safety of the path), a set of Pareto optimal paths that satisfy numerous constraints, especially the current effects will be generated for the USV.

4.1. Case studies of currents with fixed direction and speed

Within the first two cases, we set the USV's velocity v=6kn, the direction of the current θ=22 ° and the velocity of the current v_c=1kn; the sequential points on the linear left channel boundary C^L_{han} are $(-10, 5)$ and $(10, 5)$, and those on C^R_{han} are $(-10, -5)$ and $(10, -5)$. The USV navigates from $S_1(-9.5, -1)$ to $G_1(8.8, 0)$ in the first case, while it navigates from $S_1(8.8, 0)$ to $G_1(-9.5, -1)$ in the second case. The initial and final positions of the USV in the first two cases interchange with each other. The coordinate values of O_{bs} from left to right are as below.

$$O_{bs\_1} = \begin{bmatrix} -9.5 & -8.5 & -7.5 & -8.7 \\ 2.7 & 2.3 & 2.8 & 3.7 \end{bmatrix}',$$

$$O_{bs\_2} = \begin{bmatrix} -9 & -7 & -5 & -6.6 \\ -2.75 & -3.75 & -2.65 & -1.75 \end{bmatrix}',$$

$$O_{bs\_3} = \begin{bmatrix} -2.5 & -1.0 & -1.8 \\ 0 & -0.5 & 2.0 \end{bmatrix}',$$

$$O_{bs\_4} = \begin{bmatrix} 1.0 & 0.6 & 2.7 & 2.4 \\ -2.5 & -3.5 & -3.5 & -1.5 \end{bmatrix}',$$

$$O_{bs\_5} = \begin{bmatrix} 2 & 3.1 & 2.6 \\ 3 & 2 & 3.8 \end{bmatrix}',$$

$$O_{bs\_6} = \begin{bmatrix} 5.5 & 7.5 & 8.5 \\ -2.6 & -3.6 & -1.6 \end{bmatrix}',$$

$$O_{bs\_7} = \begin{bmatrix} 6 & 8.5 & 7 \\ 3.1 & 2.6 & 4 \end{bmatrix}'.$$

Accordingly, the sets of circles orderly corresponding to O_{bs} are $\{(-8.50, 2.73), 1.00\}$, $\{(-7.00, -2.66), 2.00\}$, $\{(-1.45, 0.73), 1.31\}$, $\{(1.65, -2.64), 1.36\}$, $\{(2.84, 2.90), 0.93\}$, $\{(7.00, -2.11), 1.58\}$, $\{(7.27, 2.96), 1.28\}$, respectively. The generated paths can cross with the circles that covered O_{bs}, and the corresponding safety degree of the paths can be reached by using Eq. (12).

To determine the iteration number T_{iter} of DAMOPSO, the convergency curves of cases in Section 4.1 are presented in Fig. 2 and Fig. 3, respectively. With T_{iter} increasing from 100 to 160, from 160 to 200, and from 200 to 220, the Pareto fronts are updated accordingly. Referring to the Pareto fronts, as shown in Fig. 2 and Fig. 3, there are evident differences when T_{iter} increases from 100 to 160, and from 160 to 220, while little differences exist when T_{iter} transits from 200 and 220. Consequently, it can be reached that T_{iter} in Section 4.1.1 and Section 4.1.2 both can be set to a number between 200 and 220. Following that, to low down the running time, it is feasible that the value of T_{iter} can be 200.

4.1.1. USV navigates from $(-9.5, -1)$ to $(8.8, 0)$ in currents with fixed direction and speed

In the first case, Fig. 4 presents the path planning environment, and the Pareto paths set for the USV from $(-9.5, -1)$ to $(8.8, 0)$ generated by DAMOPSO. Fig. 5 notes the shortest and most economical path, the smoothest path and the safest path. It shows that

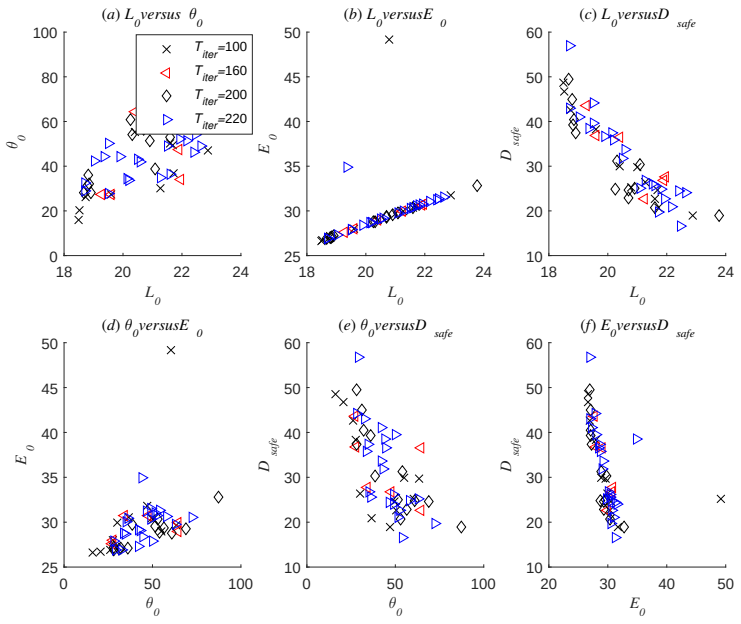

Figure 2: Convergence curves for the USV from (-9.5,-1) to (8.8,0) in currents with fixed direction and speed while iteration number T_{iter}=100, 160, 200, and 220

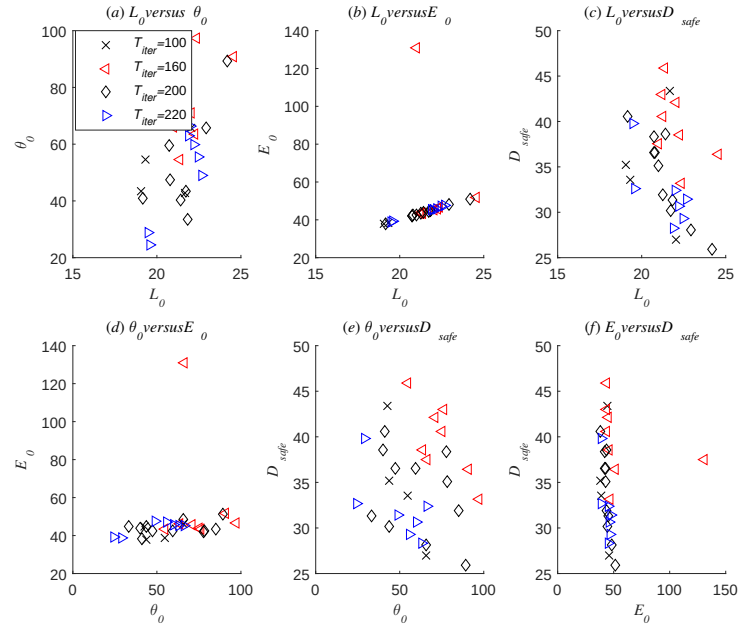

Figure 3: Convergence curves for the USV from (-9.5,-1) to (8.8,0) in currents with fixed direction and speed while iteration number T_{iter}=100, 160, 200, and 220

the shortest path and the most economical path coincide with each other, the coordinate values of the path are shown in the first line of Table 5, with L_0=18.69 and E_0=26.90. It is noteworthy that the shortest path tends to connect the initial and final positions as straight as possible, as reflected in its second and fourth parts, while the most economical path exploits the currents as much as possible in its first and third parts. The coordi-

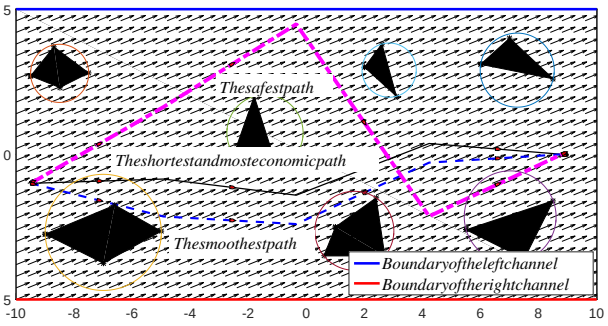

Figure 5: Three paths for the USV from (−9.5, −1) to (8.8, 0) in currents with fixed direction and speed

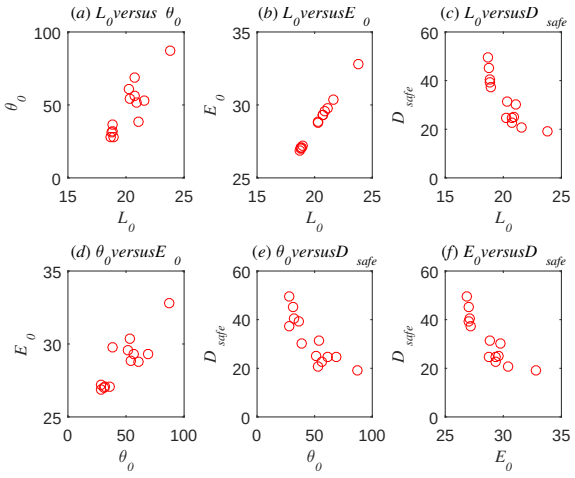

Figure 7: Two-dimensional Pareto optimality of the paths set for the USV from (-9.5,-1) to (8.8,0) in currents with fixed direction and speed

nate values of the smoothest path are given in the fifth line of Table 5, and with ζ=28.11°. Navigating with the smoothest path, the turn angle of the USV is limited to 28.11°. The coordinate values of the safest path are provided by the last line of Table 5, with D_{safe}=18.97. The safest path maintains sufficient distance to O_{bs} and owns the highest safety degree among the paths set. When it comes to the details of the paths set, Fig. 4 elaborates that the USV can explicitly take advantage of the currents in part of their path segments under multiple optimal objectives.

Table 5 shows the vaule of the optimal paths set. The maximum values of L_0, θ_0, E_0 and D_{safe} of the solutions are 27.18%, 210.52%, 21.95% and 160.67% above their corresponding best (minimum) solutions respectively. Fig. 6 shows the scatter diagram of the Pareto optimal solutions in three-dimension. The Pareto optimality of the same paths set in two-dimension is vividly depicted in Fig. 7. The correlation coefficients coe_{cor} in Fig. 7 from (a) to (f) are $coe_{cor}(L_0, \theta_0)$=0.87, $coe_{cor}(L_0, E_0)$=1.00, $coe_{cor}(L_0, D_{safe})$=−0.86, $coe_{cor}(\theta_0, E_0)$=0.87, $coe_{cor}(\theta_0, D_{safe})$=−0.85, and $coe_{cor}(E_0, D_{safe})$=−0.87. According to the value of coe_{cor}, when choosing the goal with the shortest path L_0, the obtained path would have the most economic E_0, moderate smoothness θ_0, and the lowest safety D_{safe}. If the safest path D_{safe} is achieved, the path would have the longest L_0, a relatively large θ_0 and the highest E_0. Referring to this case, if only the three objectives L_0, θ_0 and D_{safe} are selected, our path planning problem with four objectives can be optimized simultaneously. Consequently, due to the objective cuts, the computational time and resources occupied by the focused problem can be saved, in essence.

Suppose pre_{set}=[**0.2** 0.3 **0** 0.5]; then, the minimum PPV=0.27, and the corresponding path is the twelfth line of Table 5 and the black dash line of Fig. 4. Meanwhile, to confirm the highly positive relations between L_0 and E_0, set pre_{set}=[**0** 0.3 **0.2** 0.5]; we then find that the minimum PPV=0.27 and the path is also the twelfth line of Table 5. This validates that the relationships among multiple objectives presented above are effective. Consequently, by virtue of simplification and the efficiency of the selection process, the USV can select the ideal path from the paths set with ease.

4.1.2. *USV navigates from* (8.8, 0) *to* (−9.5, −1) *in currents with fixed direction and speed*

In the second case, the Pareto paths set for the USV from (8.8, 0) to (−9.5, −1) in currents with fixed direction and speed are shown in Fig. 8. Each path consists of 5 sequential line segments. Fig. 9 plots the shortest and most economical path (with L_0=19.15, and E_0=38.10), the smoothest path (with ζ = 33.45°), and the safest path (with D_{safe}=25.92), and the coordinate values of above paths are orderly listed in the first, the ninth and the eleventh line of Table 6. The shortest path and the most economical path coincide with each other. It is notable that the paths of this case are dramatically different from the paths of the first case. With the same directions of the currents, most parts of the paths in Fig. 4 take full advantage of the currents; while as displayed in Fig. 8, the directions of the paths are cross with the opposite directions of the currents with different angles.

The optimal paths set is listed in Table 6. The maximum values of L_0, θ_0, E_0 and D_{safe} of the solutions are 26.42%, 166.67%, 34.07% and 56.61% above their corresponding best (minimum) solutions, respectively. Compared with the paths set shown in Table 5, the values of E_0 in this case are evidently larger than those in the first case. Moreover, the upper and lower boundaries

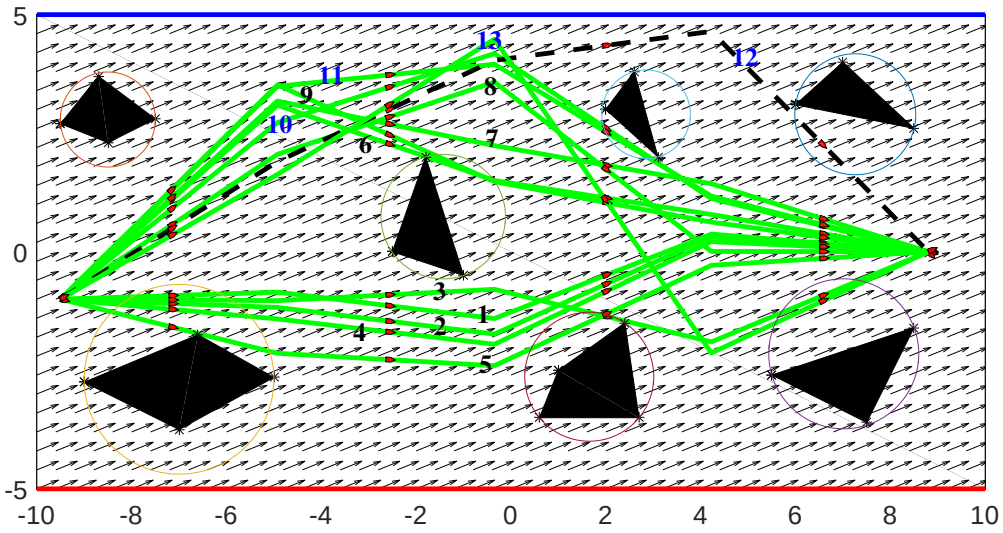

Figure 4: Generated paths for the USV from $(-9.5, -1)$ to $(8.8, 0)$ in currents with fixed direction and speed

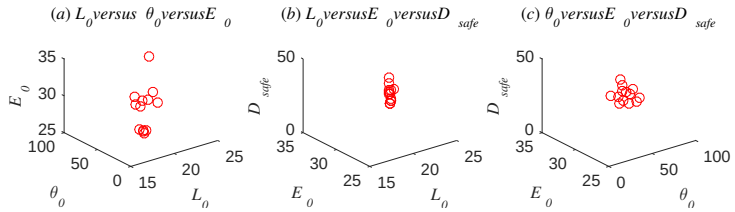

Figure 6: Three-dimensional Pareto optimality of the paths set for the USV from (-9.5,-1) to (8.8,0) in currents with fixed direction and speed

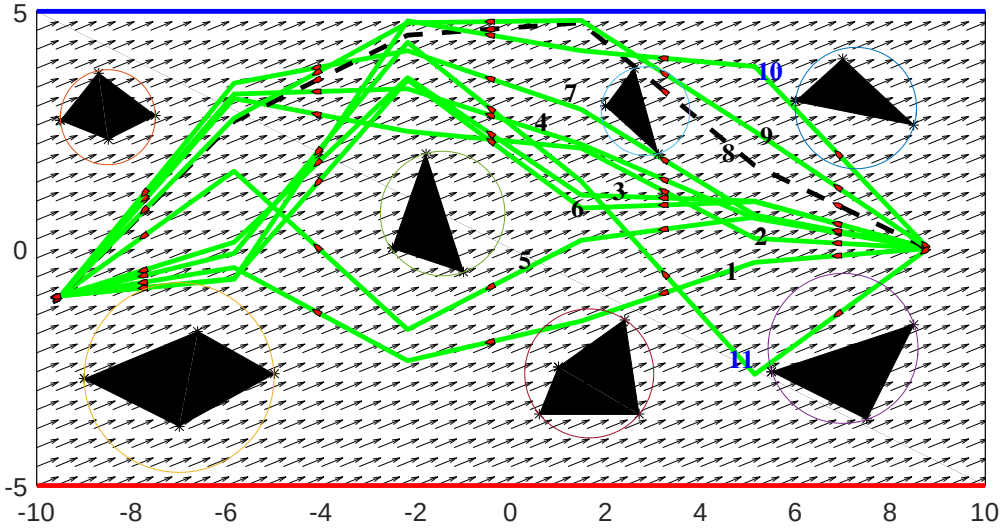

Figure 8: Generated paths for the USV from $(8.8, 0)$ to $(-9.5, -1)$ in currents with fixed direction and speed

of the four goals in the second case are larger than those in the first case. The differences are brought by the currents owing to the path direction in accordance with the currents' direction in the first case; on the contrary, the path direction crosses with the currents' direction in the second case.

Fig. 10 and Fig. 11 visualize the Pareto optimality of our achieved paths set of this case in three and two dimensions, respectively. The positive correlation coefficients are $coe_{cor}(L_0, \theta_0) = 0.39$, $coe_{cor}(L_0, E_0)$

Table 5: Optimal paths set for the USV from $(-9.5,-1)$ to $(8.8,0)$ in currents with fixed direction and speed

Paths	(x_0,y_0)	(x_1,y_1)	(x_2,y_2)	(x_3,y_3)	(x_4,y_4)	L_0(nmile)	$\theta_0(^\circ)$	E_0(h*10)	D_{Safe}(1*10)
1	**(−9.5, −1)**	**(−4.93, −0.85)**	**(−0.35, −1.41)**	**(4.23, 0.37)**	**(8.8, 0)**	**18.69**	28.20	**26.90**	49.44
2	(-9.5,-1)	(-4.93,-1.17)	(-0.35,-1.74)	(4.23,0.32)	(8.8,0)	18.79	31.17	27.02	45.02
3	(-9.5,-1)	(-4.93,-1.03)	(-0.35,-0.79)	(4.23,-1.90)	(8.8,0)	18.82	36.20	27.06	39.27
4	(-9.5,-1)	(-4.93,-1.42)	(-0.35,-1.95)	(4.23,0.22)	(8.8,0)	18.84	31.99	27.09	40.41
5	**(−9.5, −1)**	**(−4.93, −2.14)**	**(−0.35, −2.40)**	**(4.23, −0.29)**	**(8.8, 0)**	18.92	**28.11**	27.19	37.40
6	(-9.5,-1)	(-4.93,3.09)	(-0.35,1.50)	(4.23,0.79)	(8.8,0)	20.25	60.96	28.77	24.86
7	(-9.5,-1)	(-4.93,3.18)	(-0.35,2.29)	(4.23,1.44)	(8.8,0)	20.31	54.02	28.83	31.20
8	(-9.5,-1)	(-4.93,2.06)	(-0.35,3.58)	(4.23,0.01)	(8.8,0)	20.70	56.41	29.34	22.83
9	(-9.5,-1)	(-4.93,3.52)	(-0.35,1.48)	(4.23,0.62)	(8.8,0)	20.71	68.69	29.31	24.66
10	(-9.5,-1)	(-4.93,2.72)	(-0.35,4.18)	(4.23,1.12)	(8.8,0)	20.91	51.40	29.59	25.08
11	(-9.5,-1)	(-4.93,3.49)	(-0.35,3.96)	(4.23,1.17)	(8.8,0)	21.09	38.63	29.76	30.33
12	(-9.5,-1)	(-4.93,1.90)	(-0.35,4.04)	(4.23,4.65)	(8.8,0)	21.60	53.07	30.38	20.71
13	**(−9.5, −1)**	**(−4.93, 1.63)**	**(−0.35, 4.48)**	**(4.23, −2.14)**	**(8.8, 0)**	23.76	87.30	32.80	**18.97**

Table 6: Optimal paths set for the USV from $(8.8,0)$ to $(-9.5,-1)$ in currents with fixed direction and speed

Paths	(x_0,y_0)	(x_1,y_1)	(x_2,y_2)	(x_3,y_3)	(x_5,y_4)	(x_5,y_5)	L_0(nmile)	$\theta_0(^\circ)$	E_0(h*10)	D_{Safe}(1*10)
1	**(8.8, 0)**	**(5.14, −0.29)**	**(1.48, −1.53)**	**(−2.18, −2.37)**	**(−5.84, −0.40)**	**(−9.5, −1)**	**19.15**	41.08	**38.10**	40.60
2	(8.8,0)	(5.14,0.21)	(1.48,2.12)	(-2.18,2.47)	(-5.84,3.16)	(-9.5,-1)	20.74	59.40	42.24	36.55
3	(8.8,0)	(5.14,1.00)	(1.48,1.13)	(-2.18,3.60)	(-5.84,0.13)	(-9.5,-1)	20.75	77.54	42.10	38.33
4	(8.8,0)	(5.14,0.63)	(1.48,2.20)	(-2.18,3.37)	(-5.84,3.26)	(-9.5,-1)	20.81	47.57	42.44	36.56
5	(8.8,0)	(5.14,0.66)	(1.48,0.17)	(-2.18,-1.71)	(-5.84,1.63)	(-9.5,-1)	20.99	78.07	42.66	35.09
6	(8.8,0)	(5.14,0.99)	(1.48,0.85)	(-2.18,3.55)	(-5.84,-0.63)	(-9.5,-1)	21.24	85.30	43.50	31.91
7	(8.8,0)	(5.14,0.70)	(1.48,2.93)	(-2.18,4.17)	(-5.84,3.49)	(-9.5,-1)	21.39	40.20	43.92	38.57
8	(8.8,0)	(5.14,1.75)	(1.48,4.76)	(-2.18,4.50)	(-5.84,2.68)	(-9.5,-1)	21.74	43.54	44.58	30.19
9	**(8.8, 0)**	**(5.14, 2.47)**	**(1.48, 4.81)**	**(−2.18, 4.76)**	**(−5.84, 2.75)**	**(−9.5, −1)**	21.83	**33.45**	44.79	31.36
10	(8.8,0)	(5.14,3.84)	(1.48,4.17)	(-2.18,4.80)	(-5.84,-0.65)	(-9.5,-1)	22.93	65.87	48.37	28.09
11	**(8.8, 0)**	**(5.14, −2.65)**	**(1.48, 1.42)**	**(−2.18, 4.35)**	**(−5.84, −0.10)**	**(−9.5, −1)**	24.21	89.21	51.08	**25.92**

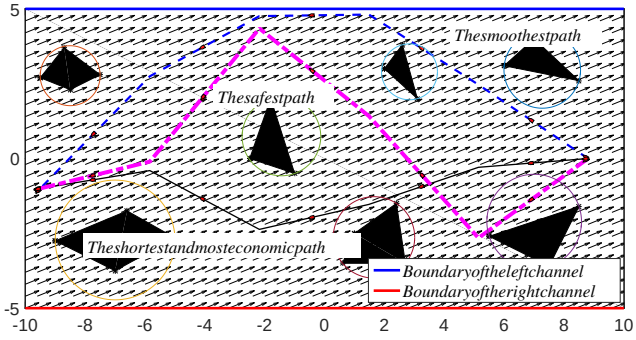

Figure 9: Three paths for the USV from $(8.8,0)$ to $(-9.5,-1)$ in currents with fixed direction and speed

$= 1.00$ and $coe_{cor}(\theta_0, E_0) = 0.39$, while the negative correlation coefficients are $coe_{cor}(L_0, D_{safe}) = -0.90$, $coe_{cor}(\theta_0, D_{safe}) = -0.36$ and $coe_{cor}(E_0, D_{safe}) = -0.89$. Referring to this case, if the path length objective and the economic cost objective need to be simultaneously optimized, it is possible to select only one goal to be optimized. Suppose pre_{set}=[**0.3** 0.2 **0** 0.5]; then, the minimum PPV=0.34, and the corresponding path is the eighth line of Table 6 and the black dash line of Fig. 8. Meanwhile, set pre_{set}=[**0** 0.2 **0.3** 0.5]; then, we find that the minimum PPV=0.33 and that the path is also the eighth line of Table 6.

The analysis shown in the first two cases demonstrates the validity and effectiveness of our multi-objective path planning model and the DAMOPSO

algorithm for USV path planning under the effects brought by currents with fixed direction and speed.

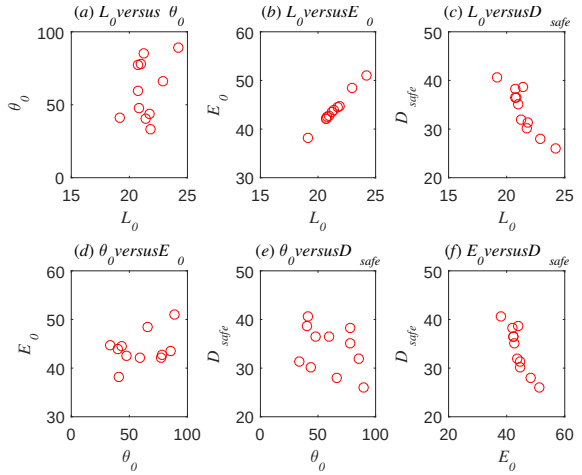

Figure 11: Two-dimensional Pareto optimality of the paths set for the USV from $(8.8, 0)$ to $(-9.5, -1)$ in currents with fixed direction and speed

4.2. Case studies in time-varying currents

Within the last two cases, the parameters related to the time-varying currents are B_0=1.2, ϵ=0.3, ω=0.4, β=π/2, k=0.84, and c=0.12. The USV's velocity v=3kn, the sequential points on C^L_{han} are $(-8, 3)$ and $(8, 3)$, and those on C^R_{han} are $(-8, -3)$ and $(8, -3)$. The USV navigates from $S_1(-7.5, 1)$ to $G_1(6.8, 1.5)$ in the third case, while it navigates from $S_1(6.8, 1.5)$ to $G_1(-7.5, 1)$ in the fourth case. This shows that the initial and final positions of the USV in the last two cases interchange with each other. The coordinate values of O_{bs} from left to right are as below.

$$O_{bs\_1} = \begin{bmatrix} -4.5 & -3 & -2.8 & -3.7 \\ 1 & 0.8 & 1.45 & 1.4 \end{bmatrix}',$$

$$O_{bs\_2} = \begin{bmatrix} -0.5 & 0.3 & 0.5 & 0 & -0.3 \\ -2.5 & -2.3 & -1.85 & -1.5 & -2 \end{bmatrix}',$$

$$O_{bs\_3} = \begin{bmatrix} 2 & 3 & 2.8 \\ 2 & 1.1 & 2.3 \end{bmatrix}'.$$

Accordingly, the sets of circles orderly corresponding to O_{bs} are $\{(-3.65, 1.22), 0.88\}$, $\{(-0.05, -2.10), 0.60\}$, $\{(2.60, 1.67), 0.69\}$, respectively.

The convergency curves of cases in Section 4.2 are presented in Fig. 12 and Fig. 13, respectively. Similar to Section 4.1, T_{iter} both can be 200 in Section 4.2.1 and Section 4.2.2.

4.2.1. USV navigates from $(-7.5, 1)$ to $(6.8, 1.5)$ in time-varying currents

For the third case, the paths set for the USV from $(-7.5, 1)$ to $(6.8, 1.5)$ in time-varying currents is given in Fig. 14, and their values are provided in Table 7. The path consists of 7 sequential line segments. Within the paths set, the maximum values of L_0, θ_0, E_0 and D_{safe} of the solutions are 28.06%, 155.47%, 65.33% and ∞ above their corresponding best (minimum) solutions respectively. Fig. 15 shows four paths including the shortest path (with L_0=15.29), the smoothest path (with ζ = 38.07°), the most economical path (with E_0 = 42.11), and the safest path (with D_{safe} = 0), and their coordinate values are sequentially stressed in bold lines of Table 7. It is worth noting that the shortest path and the smoothest path pass through the weak currents region with a lower safety degree. Headings of the most economical path and the safest path are closely approximate to the directions of the strong currents. Furthermore, the heading of the most economical path and the direction of currents overlap closely. Above phenomena shown in Fig. 14 and Fig. 15 illustrate that most of the paths in the generated paths set have made full use of the currents remarkably.

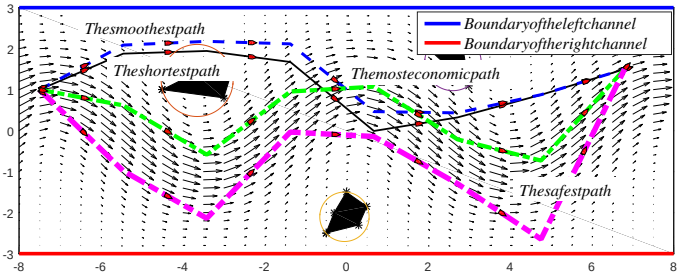

Figure 15: Four paths for the USV from (-7.5, 1.0) to (6.8, 1.5) with time-varying currents

Fig. 16 and Fig. 17 unfold three- and two-dimensional Pareto optimality of the above paths set, respectively. The positive correlation coefficients are $coe_{cor}(L_0, \theta_0)$=0.88, $coe_{cor}(L_0, E_0)$=0.73 and $coe_{cor}(\theta_0, E_0)$=0.42, while the negative correlation coefficients are $coe_{cor}(L_0, D_{safe})$=−0.78, $coe_{cor}(\theta_0, D_{safe})$=−0.63 and $coe_{cor}(E_0, D_{safe})$=−0.62. There is little relationship between the path smoothness versus the economic cost. Suppose pre_{set}=[0.1 **0.4 0** 0.5]; then, the minimum PPV=0.29, and the corresponding path is the fourth line of Table 7 and the black dash path of Fig. 14. Meanwhile, set pre_{set}=[0.1 **0 0.4** 0.5]; then, we find that the minimum PPV=0.19, and that the path is the tenth line of Table 7 and the blue dotted line of Fig. 14. Accordingly, if the USV pays equal attention to the path smoothness and the economic cost, the value of pre_2 should be as large as that of pre_3.

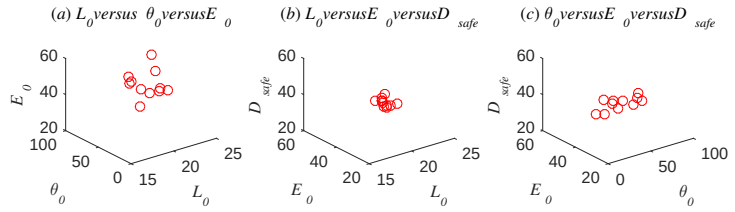

Figure 10: Three-dimensional Pareto optimality of the paths set for the USV from (8.8, 0) to (−9.5, −1) in currents with fixed direction and speed

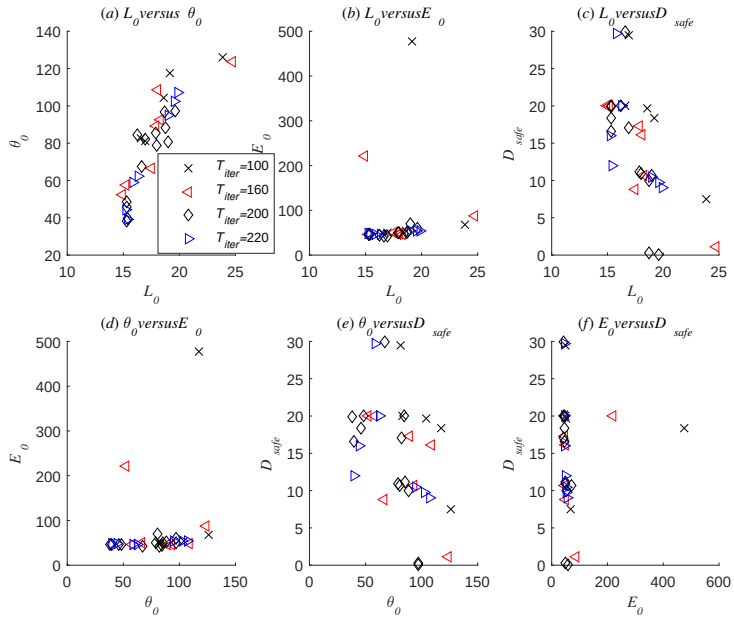

Figure 12: Convergence curves for the USV from (-7.5, 1.0) to (6.8, 1.5) with time-varying currents while iteration number T_{iter}=100, 160, 200, and 220

Table 7: Optimal paths set for the USV from (-7.5, 1) to (6.8, 1.5) in time-varying currents

Paths	(x_0, y_0)	(x_1, y_1)	(x_2, y_2)	(x_3, y_3)	(x_4, y_4)	(x_5, y_5)	(x_6, y_6)	(x_7, y_7)	L_0(nmile)	θ_0(°)	E_0(h*10)	D_{Safe}(1*10)
1	**(−7.5, 1)**	**(−5.46, 1.88)**	**(−3.41, 1.94)**	**(−1.37, 1.68)**	**(0.67, −0.01)**	**(2.71, 0.32)**	**(4.76, 0.87)**	**(6.8, 1.5)**	**15.29**	48.66	45.29	20.00
2	**(−7.5, 1)**	**(−5.46, 2.09)**	**(−3.41, 2.18)**	**(−1.37, 2.12)**	**(0.67, 0.46)**	**(2.71, 0.43)**	**(4.76, 0.88)**	**(6.8, 1.5)**	15.30	**38.07**	45.31	19.86
3	(-7.5,1)	(-5.46,2.09)	(-3.41,2.34)	(-1.37,2.32)	(0.67,0.57)	(2.71,0.75)	(4.76,1.07)	(6.8,1.5)	15.32	45.93	45.78	18.41
4	(-7.5,1)	(-5.46,2.34)	(-3.41,2.44)	(-1.37,2.48)	(0.67,0.89)	(2.71,0.94)	(4.76,1.59)	(6.8,1.5)	15.36	39.66	46.03	16.59
5	(-7.5,1)	(-5.46,1.12)	(-3.41,0.82)	(-1.37,0.02)	(0.67,0.84)	(2.71,0.55)	(4.76,-0.89)	(6.8,1.5)	16.21	84.60	43.70	20.00
6	**(−7.5, 1)**	**(−5.46, 0.62)**	**(−3.41, −0.59)**	**(−1.37, 0.95)**	**(0.67, 1.08)**	**(2.71, −0.21)**	**(4.76, −0.73)**	**(6.8, 1.5)**	16.60	67.48	**42.11**	29.99
7	(-7.5,1)	(-5.46,0.13)	(-3.41,-0.83)	(-1.37,0.49)	(0.67,0.56)	(2.71,-0.24)	(4.76,-1.33)	(6.8,1.5)	16.95	82.22	42.60	17.11
8	(-7.5,1)	(-5.46,-0.41)	(-3.41,-1.82)	(-1.37,-1.37)	(0.67,1.52)	(2.71,0.31)	(4.76,2.17)	(6.8,1.5)	17.87	85.24	49.51	11.15
9	(-7.5,1)	(-5.46,-0.96)	(-3.41,-1.88)	(-1.37,-0.63)	(0.67,1.59)	(2.71,2.93)	(4.76,0.85)	(6.8,1.5)	17.99	78.68	50.44	10.91
10	(-7.5,1)	(-5.46,-0.49)	(-3.41,-1.63)	(-1.37,0.10)	(0.67,0.16)	(2.71,-0.89)	(4.76,-2.32)	(6.8,1.5)	18.71	96.85	49.73	0.27
11	(-7.5,1)	(-5.46,-1.24)	(-3.41,-2.19)	(-1.37,-0.97)	(0.67,1.18)	(2.71,2.79)	(4.76,0.37)	(6.8,1.5)	18.73	88.20	52.55	10.00
12	(-7.5,1)	(-5.46,-1.29)	(-3.41,-2.17)	(-1.37,-1.39)	(0.67,1.69)	(2.71,2.91)	(4.76,0.50)	(6.8,1.5)	18.99	80.64	69.63	10.67
13	**(−7.5, 1)**	**(−5.46, −0.98)**	**(−3.41, −2.14)**	**(−1.37, −0.03)**	**(0.67, −0.14)**	**(2.71, −1.29)**	**(4.76, −2.65)**	**(6.8, 1.5)**	19.59	97.27	59.76	**0**

4.2.2. USV navigates from (6.8, 1.5) *to* (−7.5, 1) *in time-varying currents*

For the fourth case, Fig. 18 shows all the paths generated by DAMOPSO algorithm. Each path consists of

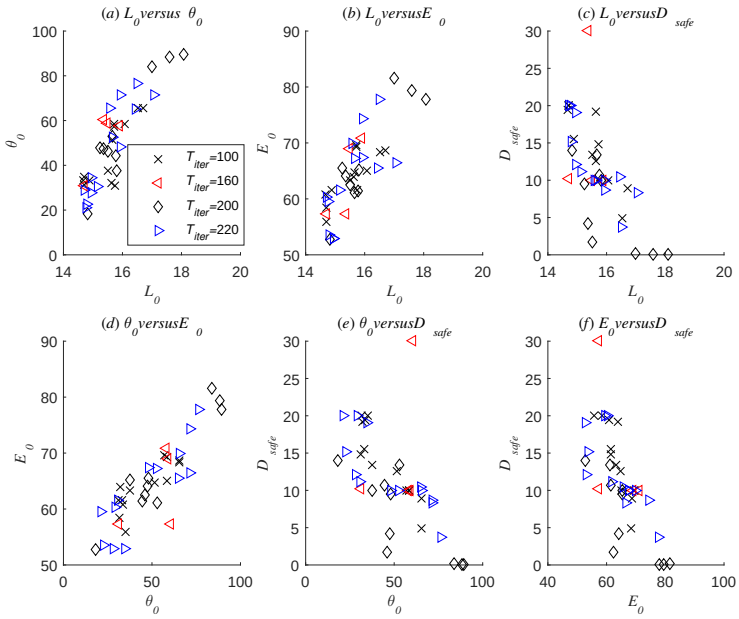

Figure 13: Convergence curves for the USV from (6.8, 1.5) to (-7.5, 1.0) with time-varying currents while iteration number T_{iter}=100, 160, 200, and 220

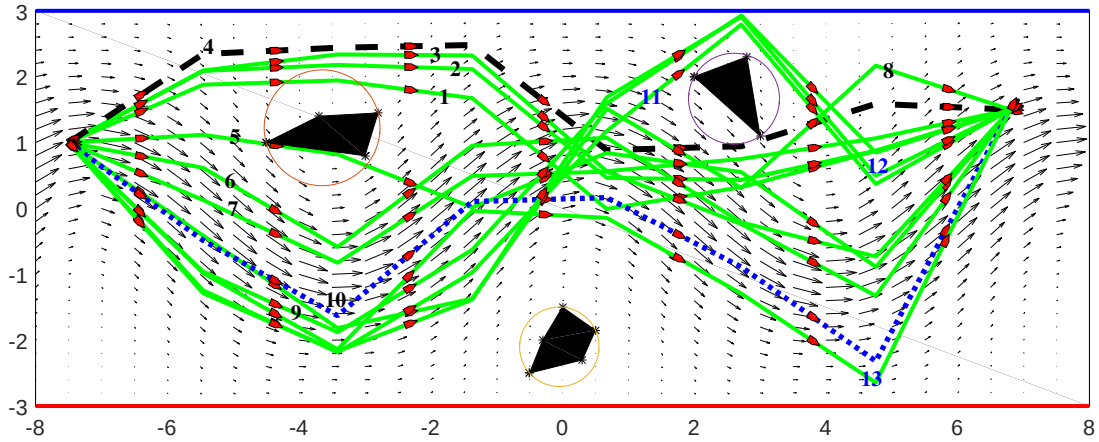

Figure 14: Generated paths for the USV from (-7.5, 1.0) to (6.8, 1.5) with time-varying currents

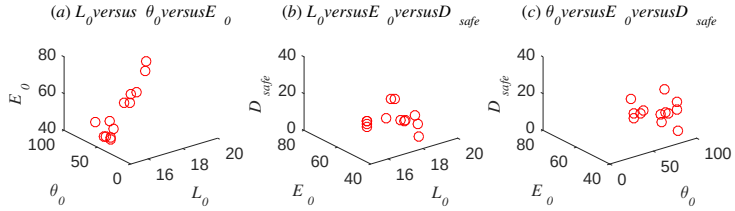

Figure 16: Three-dimensional Pareto optimality of the paths set for the USV from (-7.5, 1.0) to (6.8, 1.5) with time-varying currents

5 sequential line segments. Fig. 19 offers three paths: the shortest, smoothest and most economical path (with L_0=14.81, ζ=18.35° and E_0=52.68), and two safest paths (with D_{safe}=0). The shortest path, the smoothest path and the most economical path coincide with each other. And the paths shown in Fig. 19 are emphasized in bold lines in sequence. It is notable that the three generated paths are dramatically different from the paths

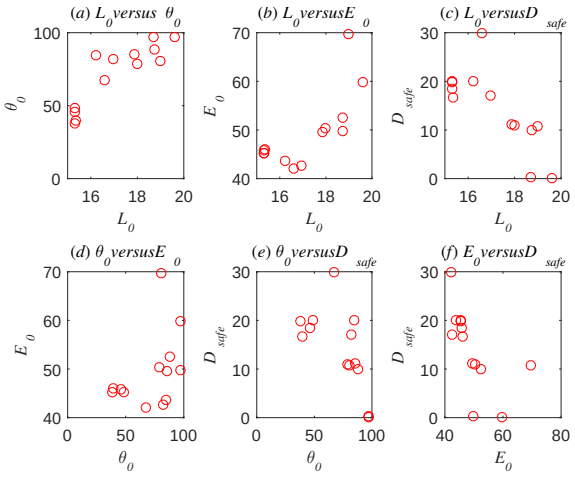

Figure 17: Two-dimensional Pareto optimality of the paths set with four objectives for the USV from (-7.5, 1.0) to (6.8, 1.5) with time-varying currents

in Fig. 15. The heading of the paths in Fig. 18 coincide with the reverse directions of the strong currents, while in Fig. 14, the paths with the goals of economic cost and safety almost follow the directions of the strong currents. The maximum values of L_0, θ_0, E_0 and D_{safe} of the solutions are 22.12%, 387.14%, 54.83% and ∞ above their corresponding best (minimum) solutions respectively. Compared with the paths set shown in Table 7, the interval value of the economic cost in this case is evidently larger than that in the third case. This case verifies that, when the USV is voyaging in counter currents, the economic cost of the USV increases in general.

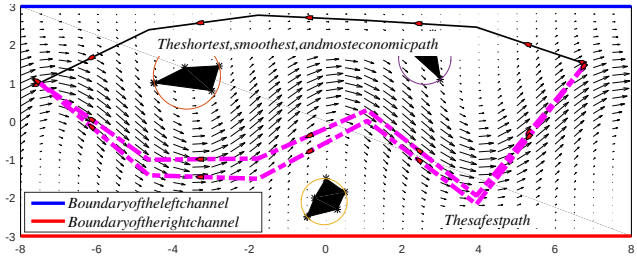

Figure 19: Three paths for the USV from (6.8, 1.5) to (-7.5, 1.0) with time-varying currents

Fig. 20 and Fig. 21 depict the Pareto optimality of the paths set in three-dimension and two-dimension, respectively. The positive correlation coefficients are $coe_{cor}(L_0, \theta_0) = 0.94$, $coe_{cor}(L_0, E_0) = 0.90$ and $coe_{cor}(\theta_0, E_0) = 0.95$, while the negative correlation coefficients are $coe_{cor}(L_0, D_{safe}) = -0.74$, $coe_{cor}(\theta_0, D_{safe}) = -0.80$ and $coe_{cor}(E_0, D_{safe}) = -0.82$. In this case, if the two objectives with positive coe_{cor} need to be simultaneously optimized, it is reasonable and feasible to optimize any one of the two objectives. L_0 and θ_0 are selected for optimizing at the same time. Suppose pre_{set}=[**0.5 0** 0 0.5]; then, the minimum PPV=0.17, and the corresponding path is the fourth line of Table 8 and the blue dash path of Fig. 18. Meanwhile, set pre_{set}=[**0 0.5** 0 0.5]; then, the minimum PPV=0.26 and that the path is also the fourth line of Table 8. However, if the two objectives with negative coe_{cor} need to be simultaneously optimized, it needs to optimize them equally. Referring to E_0 and D_{safe}, if pre_{set}=[0.5 0.2 **0 0.3**], then minimum PPV=0.16 and the corresponding path is the fourth line of Table 8. If pre_{set}=[0.5 0.2 **0.3 0**], the minimum PPV=0 and the corresponding path is the first line of Table 8 and the black dotted line of Fig. 18.

The analysis shown in the last two cases illustrates that, by using our path planning model and the DAMOPSO algorithm, the Pareto optimal paths set is achieved for the USV in the environment with time-varying currents.

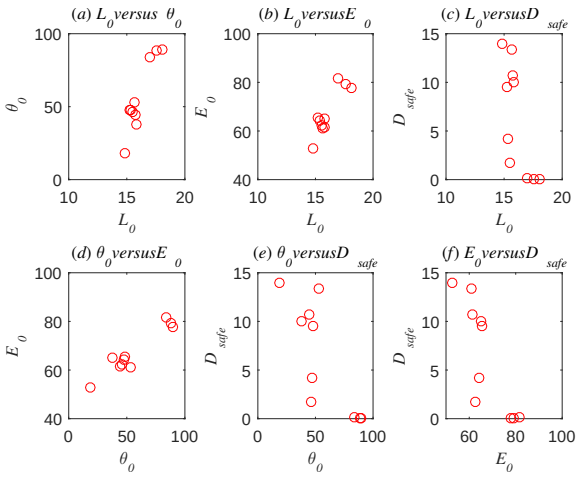

Figure 21: Two-dimensional Pareto optimality of the paths set with four objectives for the USV from (6.8, 1.5) to (-7.5, 1.0) with time-varying currents

5. Conclusions

This paper has comprehensively studied the multi-objective path planning problem for USVs in environments with currents effects. Our focused path planning problem tends to simultaneously optimize four objectives (the path length, the path smoothness, the economic cost and the path safety) while is subject to the collision avoidance, motion boundaries and currents effects. A multi-objective nonlinear optimization model with many constraints has been formulated, and its characteristics have been analyzed. The DAMOPSO algo-

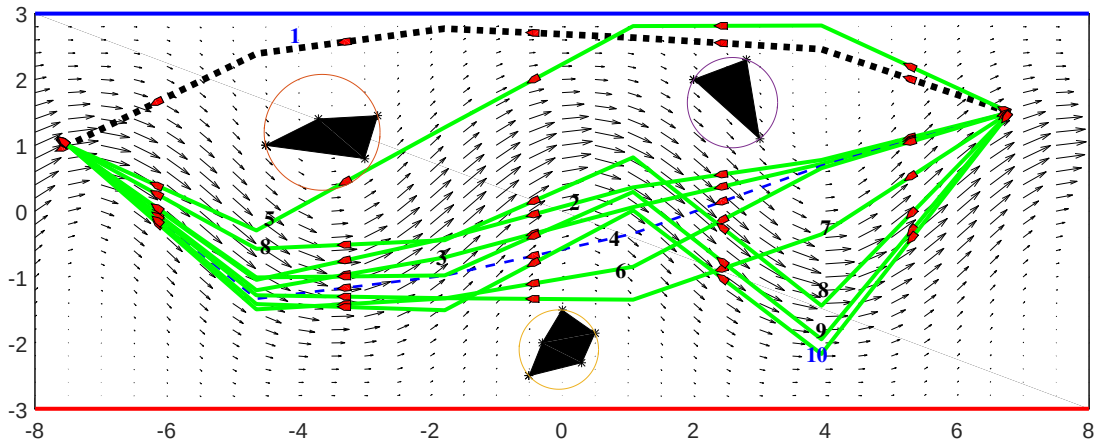

Figure 18: Generated paths for the USV from (6.8, 1.5) to (-7.5, 1.0) with time-varying currents

Table 8: Optimal paths set for the USV from (6.8,1.5) to (-7.5,1) in time-varying currents

Paths	(x_0, y_0)	(x_1, y_1)	(x_2, y_2)	(x_3, y_3)	(x_4, y_4)	(x_5, y_5)	L_0(nmile)	θ_0(°)	E_0(h*10)	D_{Safe}(1*10)
1	**(6.8, 1.5)**	**(3.94, 2.46)**	**(1.08, 2.64)**	**(−1.78, 2.77)**	**(−4.64, 2.39)**	**(−7.5, 1)**	**14.81**	**18.35**	**52.68**	13.94
2	(6.8,1.5)	(3.94,0.78)	(1.08,0.36)	(-1.78,-0.41)	(-4.64,-1.04)	(-7.5,1)	15.25	47.94	65.49	9.48
3	(6.8,1.5)	(3.94,0.72)	(1.08,0.06)	(-1.78,-0.70)	(-4.64,-1.2)	(-7.5,1)	15.37	47.47	64.1	4.18
4	(6.8,1.5)	(3.94,0.69)	(1.08,-0.34)	(-1.78,-0.98)	(-4.64,-1.33)	(-7.5,1)	15.51	46.16	62.49	1.75
5	(6.8,1.5)	(3.94,2.82)	(1.08,2.81)	(-1.78,1.27)	(-4.64,-0.29)	(-7.5,1)	15.66	52.99	61.03	13.35
6	(6.8,1.5)	(3.94,0.65)	(1.08,-0.84)	(-1.78,-1.32)	(-4.64,-1.49)	(-7.5,1)	15.77	44.38	61.42	10.7
7	(6.8,1.5)	(3.94,-0.35)	(1.08,-1.34)	(-1.78,-1.32)	(-4.64,-1.28)	(-7.5,1)	15.81	37.64	65.26	10.0
8	(6.8,1.5)	(3.94,-1.44)	(1.08,0.82)	(-1.78,-0.44)	(-4.64,-0.57)	(-7.5,1)	16.99	83.97	81.57	0.16
9	**(6.8, 1.5)**	**(3.94, −1.95)**	**(1.08, 0.29)**	**(−1.78, −0.97)**	**(−4.64, −1.00)**	**(−7.5, 1)**	17.59	88.35	79.33	**0**
10	**(6.8, 1.5)**	**(3.94, −2.17)**	**(1.08, 0.01)**	**(−1.78, −1.50)**	**(−4.64, −1.41)**	**(−7.5, 1)**	18.09	89.38	77.81	**0**

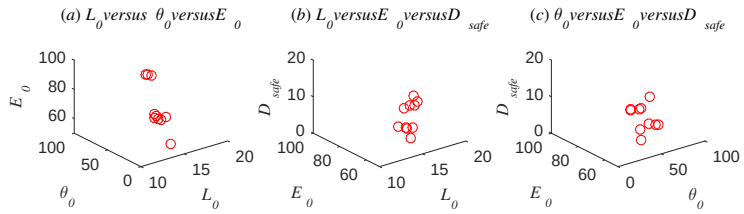

Figure 20: Three-dimensional Pareto optimality of the paths set for the USV from (6.8, 1.5) to (-7.5, 1.0) with time-varying currents

rithm has been introduced to resolve our formulated USV path planning model, which consists of a PSO module, intelligent search method module, archive and leader dynamic update module, and path selection strategy. After generous comparison with nine competitive MOO algorithms on nineteen multi-objective benchmark problems, excellent performance of DAMOPSO is verified in terms of epsilon indicator $I^1_{\varepsilon+}$, spread Δ, and hypervolume HV. With DAMOPSO, a set of Pareto optimal paths for a USV with numerous combinations of the four objectives has been generated. Following that, the USV would select an ideal path from the paths set by balancing the four objectives to its requirements. Computational simulations under numerous scenarios validate the effective applications of our path planning model and the DAMOPSO algorithm.

In the near future, the following interesting studies could be conducted in-depth. At first, we will apply our approach to USV path planning experiments in coastal regions with current effects. Moreover, other environmental effects including the waves also could be considered in our formulated path planning model; then,

the achieved paths set would be more practical for USV navigation. Finally, it would be valuable to fulfill the multiple USVs path planning problem with various environmental effects based on our model.

References

[1] Tam, C., Bucknall, R.. Cooperative path planning algorithm for marine surface vessels. Ocean Eng 2013;57:25–33.

[2] Liu, Y., Bucknall, R.. Path planning algorithm for unmanned surface vehicle formations in a practical maritime environment. Ocean Eng 2015;97:126–44.

[3] Ma, Y., Zhao, Y., Diao, J., Gan, L., Bi, H., Zhao, J.. Design of sail-assisted unmanned surface vehicle intelligent control system. Math Probl Eng 2016;2016:1–13.

[4] Liu, Y., Bucknall, R.. The angle guidance path planning algorithms for unmanned surface vehicle formations by using the fast marching method. Appl Ocean Res 2016;59:327–344.

[5] Nadj, D., Mivskovic, N., Mandic, F.. Navigation, guidance and control of an overactuated marine surface vehicle. Annu Rev Control 2015;40:172–81.

[6] Perera, L.P., Ferrari, V., Santos, F.P., Hinostroza, M.A., Soares, C.G.. Experimental evaluations on ship autonomous navigation and collision avoidance by intelligent guidance. IEEE J Ocean Eng 2015;40(2):374–87.

[7] Zheng, E.H., Xiong, J.J., Luo, J.L.. Second order sliding mode control for a quadrotor uav. ISA Trans 2014;53(4):1350–6.

[8] Ma, Y., Wang, H., Xie, Y., Guo, M.. Path planning for multiple mobile robots under double-warehouse. Inform Sci 2014;278:357–79.

[9] Zhang, B., Tang, L., DeCastro, J., Roemer, M.J., Goebel, K.. A recursive receding horizon planning for unmanned vehicles. IEEE Trans Ind Electron 2015;62(5):2912–20.

[10] Roberge, V., Tarbouchi, M., Labonté, G.. Comparison of parallel genetic algorithm and particle swarm optimization for real-time uav path planning. IEEE Trans Ind Inform 2013;9(1):132–41.

[11] Babel, L., Zimmermann, T.. Planning safe navigation routes through mined waters. Eur J Operat Res 2015;241(1):99–108.

[12] Wang, Y., Wang, S., Tan, M.. Path generation of autonomous approach to a moving ship for unmanned vehicles. IEEE Trans Ind Electron 2015;62(9):5619–29.

[13] Zhang, G., Zhang, X.. A novel dvs guidance principle and robust adaptive path-following control for underactuated ships using low frequency gain-learning. ISA Trans 2015;56:75–85.

[14] Kuwata, Y., Wolf, M.T., Zarzhitsky, D., Huntsberger, T.L.. Safe maritime autonomous navigation with colregs, using velocity obstacles. IEEE J Ocean Eng 2014;39(1):110–9.

[15] Yoo, B., Kim, J.. Path optimization for marine vehicles in ocean currents using reinforcement learning. J Mar Sci Technol 2015;:1–10.

[16] Subramani, D.N., Lermusiaux, P.F.. Energy-optimal path planning by stochastic dynamically orthogonal level-set optimization. Ocean Model 2016;100:57–77.

[17] Wolek, A., Cliff, E.M., Woolsey, C.A.. Energy-optimal paths for a glider with speed and load factor controls. J Guid Control Dyn 2015;39(2):1–9.

[18] Lee, T., Kim, H., Chung, H., Bang, Y., Myung, H.. Energy efficient path planning for a marine surface vehicle considering heading angle. Ocean Eng 2015;107:118–31.

[19] Alvarez, A., Caiti, A., Onken, R.. Evolutionary path planning for autonomous underwater vehicles in a variable ocean. IEEE J Ocean Eng 2004;29(2):418–29.

[20] Ma, Y., Wang, H., Zamirian, M.. A novel approach for multiple mobile objects path planning: Parametrization method and conflict resolution strategy. Phys Lett A 2012;376(4):377–86.

[21] Ma, Y., Zamirian, M., Yang, Y., Xu, Y., Zhang, J.. Path planning for mobile objects in four-dimension based on particle swarm optimization method with penalty function. Math Probl Eng 2013;2013:1–9.

[22] Campbell, S., Naeem, W., Irwin, G.. A review on improving the autonomy of unmanned surface vehicles through intelligent collision avoidance manoeuvres. Annu Rev Control 2012;36:267–83.

[23] Han, D.H., Kim, Y.D., Lee, J.Y.. Multiple-criterion shortest path algorithms for global path planning of unmanned combat vehicles. Comput Ind Eng 2014;71:57–69.

[24] Fossen, T.I.. Handbook of marine craft hydrodynamics and motion control. John Wiley & Sons; 2011.

[25] Naeem, W., Irwin, G.W., Yang, A.. Colregs-based collision avoidance strategies for unmanned surface vehicles. Mechatron 2012;22(6):669–78.

[26] Yan, Z., Yan, X., Ma, F., Chu, X.. Green yangtze river, intelligent shipping information system and its key technologies. J Transp Inform Saf 2010;29:76–81.

[27] Sun, X., Yan, X., Wu, B., Song, X.. Analysis of the operational energy efficiency for inland river ships. Transp Res Part D: Transp Enviro 2013;22:34–9.

[28] Pristrom, S., Yang, Z., Wang, J., Yan, X.. A novel flexible model for piracy and robbery assessment of merchant ship operations. Reliab Eng Sys Saf 2016;155:196–211.

[29] Fu, S., Zhang, D., Montewka, J., Yan, X., Zio, E.. Towards a probabilistic model for predicting ship besetting in ice in arctic waters. Reliab Eng Sys Saf 2016;155:124–36.

[30] Zhang, Y., Gong, D.w., Zhang, J.h.. Robot path planning in uncertain environment using multi-objective particle swarm optimization. Neurocomputing 2013;103:172–85.

[31] Corbera, S., Olazagoitia, J.L., Lozano, J.A.. Multi-objective global optimization of a butterfly valve using genetic algorithms. ISA Trans 2016;63:401–12.

[32] Tang, Y., Wang, Z., Fang, J.. Feedback learning particle swarm optimization. Appl Soft Comput 2011;11(8):4713–25.

[33] Tang, Y., Gao, H., Kurths, J., Fang, J.a.. Evolutionary pinning control and its application in uav coordination. IEEE Trans Ind Inform 2012;8(4):828–38.

[34] Du, W., Leung, S.Y.S., Tang, Y., Vasilakos, A.V.. Differential evolution with event-triggered impulsive control. IEEE Trans Cybern 2017;47(1):244–57.

[35] Goh, C.K., Tan, K.C., Liu, D., Chiam, S.C.. A competitive and cooperative co-evolutionary approach to multi-objective particle swarm optimization algorithm design. Eur J Operat Res 2010;202(1):42–54.

[36] Fossen, T.I.. Marine control systems: guidance, navigation and control of ships, rigs and underwater vehicles. Trondheim, Norway: Marine Cybernetics; 2002.

[37] Liu, L., Wang, D., Peng, Z.. Coordinated path following of multiple underacutated marine surface vehicles along one curve. ISA Trans 2016;64:258–68.

[38] Soulignac, M.. Feasible and optimal path planning in strong current fields. IEEE Trans Robot 2011;27(1):89–98.

[39] Eichhorn, M.. Optimal routing strategies for autonomous underwater vehicles in time-varying environment. Robot Auton Syst 2015;67:33–43.

[40] Michael, R.G., Johnson, D.S.. Computers and intractability: A guide to the theory of np-completeness. WH Free Co, San Fr 1979;:90–1.

[41] Liu, S., Sun, D., Zhu, C.. Coordinated motion planning for multiple mobile robots along designed paths with formation re-

quirement. IEEE Trans Mechatron 2011;16(6):1021–31.
[42] Guo, Y., Parker, L.. A distributed and optimal motion planning approach for multiple mobile robots. In: IEEE International Conference on Robotics and Automation. IEEE; 2002, p. 2612–9.
[43] Li, X.. A non-dominated sorting particle swarm optimizer for multiobjective optimization. In: Genet. Evol. Comput. Conf. Springer; 2003, p. 198–198.
[44] Coello, C.A.C., Pulido, G.T., Lechuga, M.S.. Handling multiple objectives with particle swarm optimization. IEEE Trans Evolut Comput 2004;8(3):256–79.
[45] Tripathi, P.K., Bandyopadhyay, S., Pal, S.K.. Multi-objective particle swarm optimization with time variant inertia and acceleration coefficients. Inf Sci (Ny) 2007;177(22):5033–5049.
[46] Daneshyari, M., Yen, G.G.. Cultural-based multiobjective particle swarm optimization. IEEE Trans Syst Man, Cybern Part B 2011;41(2):553–567.
[47] Juang, C., Chang, Y.. Evolutionary-group-based particle-swarm-optimized fuzzy controller with application to mobile-robot navigation in unknown environments. IEEE Trans Fuzzy Sys 2011;19(2):379–92.
[48] Jafari-Marandi, R., Hu, M., Omitaomu, O.A.. A distributed decision framework for building clusters with different heterogeneity settings. Appl Energy 2016;165:393–404.
[49] Cummings, M.L., Marquez, J.J., Roy, N.. Human-automated path planning optimization and decision support. Int J Hum-Comput 2012;70(2):116–28.
[50] Durillo, J.J., García-Nieto, J., Nebro, A.J., Coello, C.A.C., Luna, F., Alba, E.. Multi-objective particle swarm optimizers: An experimental comparison. In: 5th Int. Conf. EMO 2009. Springer; 2009, p. 495–509.
[51] Deb, K., Pratap, A., Agarwal, S., Meyarivan, T.. A fast and elitist multiobjective genetic algorithm: Nsga-ii. IEEE Trans Evolut Comput 2002;6(2):182–97.
[52] Nebro, A.J., Luna, F., Alba, E., Dorronsoro, B., Durillo, J.J., Beham, A.. Abyss: Adapting scatter search to multiobjective optimization. IEEE Trans Evol Comput 2008;12(4):439–457.
[53] Durillo, J.J., Nebro, A.J., Luna, F., Alba, E.. Solving three-objective optimization problems using a new hybrid cellular genetic algorithm. In: PPSN. Springer; 2008, p. 661–670.
[54] Zapotecas Martínez, S., Coello Coello, C.A.. A multi-objective particle swarm optimizer based on decomposition. In: Proc. 13th Annu. Conf. Genet. Evol. Comput. (GECCO 11). ACM; 2011, p. 69–76.
[55] Nebro, A.J., Durillo, J.J., Luna, F., Dorronsoro, B., Alba, E.. Mocell: A cellular genetic algorithm for multiobjective optimization. Int J Intell Syst 2009;24(7):726–746.
[56] Nebro, A.J., Durillo, J.J., Machin, M., Coello, C.A.C., Dorronsoro, B.. A study of the combination of variation operators in the nsga-ii algorithm. In: Lect. Notes Comput. Sci. Springer; 2013, p. 269–278.
[57] Sierra, M.R., Coello, C.C.. Improving pso-based multi-objective optimization using crowding, mutation and e-dominance. In: Evol. multi-criterion Optim. Springer; 2005, p. 505–519.
[58] Zitzler, E., Laumanns, M., Thiele, L.. Spea2: Improving the strength pareto evolutionary algorithm. In: Evol. Methods Des.Optim. Control with Appl. to Ind. Probl. Springer; 2001, p. 95–100.
[59] García, S., Molina, D., Lozano, M., Herrera, F.. A study on the use of non-parametric tests for analyzing the evolutionary algorithms behaviour: a case study on the cec2005 special session on real parameter optimization. J Heuristics 2009;15(6):617–644.
[60] Cummings, M.L., Buchin, M., Carrigan, G., Donmez, B.. Supporting intelligent and trustworthy maritime path planning decisions. Int J Hum-Comput 2010;68(10):616–26.
[61] Gal, O.. Unified approach of unmanned surface vehicle navigation in presence of waves. J Robot 2011;2011:1–8.

LaTeX Source Files

Click here to download LaTeX Source Files: elsarticle.cls

bst

Click here to download LaTeX Source Files: model3-num-names.bst